

https://dspace.org/

Elemental radiography using fast neutron beams

Guzek, Jacek

2012-04-11
http://hdl.handle.net/10539/11454

Downloaded from a DSpace repository. https://dspace.org/

The copyright of the above-mentioned described thesis rests with the author or the University to which it was submitted. No portion of the text derived from it may be published without the prior written consent of the author or University (as may be appropriate). *Short quotations may be included in the text of a thesis* or dissertation for purposes of illustration, comment or criticism, provided full acknowledgement is made of the source, author and University.

ELEMENTAL RADIOGRAPHY USING FAST NEUTRON BEAMS

by

JACEK GUZEK

submitted in accordance with the requirements

for the degree of

DOCTOR OF PHILOSOPHY

in the subject

PHYSICS

at the

UNIVERSITY OF THE WITWATERSRAND

PROMOTER: PROF. J I W WATTERSON

MARCH 1999

ACKNOWLEDGMENTS

First and foremost, I would like to thank my promoter, Prof. J I W Watterson for his guidance and assistance during this study.

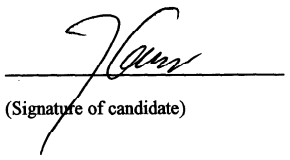
A great debt of gratitude is owed to the late Dr W R McMurray from National Accelerator Centre, for his assistance, friendship and willingness to share his vast knowledge and experience in the field of neutron physics. Without his involvement and critical approach many of the exciting experiments would not have been done.

A special note of thanks is directed to Dr U A S Tapper from DebTech, my project manager at the time, whose drive and management style facilitated this work. In addition, I would like to thank him for making a significant contribution to my personal development beyond the requirements of professional relationship. I would also like to thank the rest of the project team at DebTech for their ongoing assistance and especially G. High for proofreading. Next I would like to thank the management at DebTech for financial assistance during this study.

In addition to people mentioned above, the following people have made significant contributions to my understanding and to the output of this study. I would therefore like to thank Dr C B Franklyn from Atomic Energy Corporation, for invaluable assistance in many experiments as well as in depth discussions, Dr G. Pfister from University of Stuttgart, for sharing his vast knowledge of radiation transport calculations and modelling, Dr R C Lanza from Massachusetts Institute of Technology, for his support and many inspiring discussions and Dr R Hamm from AccSys Technology, for sharing his knowledge of modern particle accelerators. A special note of thanks is directed to Mr B Schmitt and Mr K Springhorn from National Accelerator Centre, whose willing assistance and knowledge of the operation of the Van de Graaff accelerator and nuclear electronics made many of the experiments reported in this thesis possible.

This work is dedicated to my Mother, who is fighting a battle against liver cancer, in hope that some data presented in this thesis can be used in development of effective treatment for this cruel disease.

I declare that this thesis is my own, unaided work. It is being submitted for the Degree of Doctor of Philosophy in the University of the Witwatersrand, Johannesburg. It has not been submitted before for any degree or examination in any other University.



(Signature of candidate)

The Fourth day of March 1999

ABSTRACT

The objective of this project was to investigate the physics of neutron production and their interactions with matter in order to develop an effective solution for the rapid non-destructive examination of large objects using fast neutron radiography. An additional requirement was that the technique being developed was to be applied on-line in an industrial environment. This requirement placed severe restrictions on the physical dimensions of the neutron source. Therefore, the selected neutron-producing nuclear reactions, that may potentially be employed in a robust and compact, yet prolific, fast neutron source, were investigated at low incident particle energies ($E \leq 10$ MeV). The following groups of nuclear reactions were characterised in detail: (d,n) reactions in beryllium and lithium, (p,n) reactions in beryllium and lithium and (D,D) reaction in gaseous targets.

The (d,n) reactions are very prolific and produce several neutron groups due to their large positive Q-values. Consequently, the thick target neutron spectra are complex and extend from zero to high neutron energies. The neutron production is accompanied by cascades of gamma-rays whose intensity significantly exceeds the intensity of neutron beams.

The (p,n) reactions, although not as prolific as the (d,n) reactions in the energy range considered, produce quasi mono-energetic neutron beams, which may be used in applications requiring more precise definition of the neutron energy. The associated gamma-ray production matches the neutron production in intensity. Due to the negative Q-values of the (p,n) reactions higher incident proton energies are required in order to produce neutrons with higher energies, compared with the (d,n) reactions.

The (D,D) reaction produces true mono-energetic neutron beams up to energies of 8 MeV with minimal gamma-ray component. The major challenge in utilisation of this reaction is the design of the target, which must be in the gaseous form for maximum neutron output. Two solutions are presented in this thesis namely, a windowed target with cooled gas and a differentially pumped target with a rotating seal. The windowed target is beam power limited and can tolerate up to 200 W of accelerated particle beam power. The differentially pumped target is free from this limitation and operates at up to 3.5 bar of target gas pressure. The (D,D) reaction-based neutron source utilises the differentially pumped gas target with a rotating seal is an ideal source for neutron-energy-sensitive applications.

An analytical model of dual energy fast neutron radiography for detection of an object within a mineral matrix was developed. This model examines the stochastic limits imposed by the Poisson statistics of the neutron detection process. The model was verified experimentally and the feasibility of fast neutron radiography for the detection of objects within mineral matrix was proven. This resulted in the development of the accelarator-based fast neutron source experimental facility, which was comprehensively characterised in this thesis.

TABLE OF CONTENTS

ACKNOWLEDGMENTS 2

ABSTRACT 3

TABLE OF CONTENTS 4

1. INTRODUCTION 8
   1.1 Applications of Neutron Physics 9
      1.1.1 Bulk Material Analysis 9
      1.1.2 Detection of Substances 10
      1.1.3 Medical Applications 10
      1.1.4 Imaging 11
   1.2 Outline of This Thesis 13

2. NEUTRON SOURCES 15
   2.1 Radioisotopes 15
   2.2 Nuclear Reactions 15
   2.3 Accelerator-based Sources 16

3. EXPERIMENTAL METHOD 22
   3.1 Time-of-flight Technique 22
   3.2 Response and Efficiency of Detectors 23
   3.3 Data Treatment 26

4. CHARACTERIZATION OF $^{9}Be(d,n)^{10}B$ AND $^{7}Li(d,n)^{8}Be$ REACTIONS 27
   4.1 $^{9}Be(d,n)^{10}B$ 27

      4.1.1 Neutron Production 28
      4.1.2 Gamma-ray Production 33
      4.1.3 Conclusions 34
   4.2 $^{7}Li(d,n)^{8}Be$ 35
      4.2.1 Neutron Production 35
      4.2.2 Gamma-ray Production 39
      4.2.3 Conclusions 40

5. CHARACTERIZATION OF $^{9}Be(p,n)^{9}B$ AND $^{7}Li(p,n)^{7}Be$ REACTIONS 41
   5.1 $^{9}Be(p,n)^{9}B$ 41
      5.1.1 Neutron Production 42
      5.1.2 Gamma-ray Production 48
      5.1.3 Conclusions 50
   5.2 $^{7}Li(p,n)^{7}Be$ 51
      5.2.1 Neutron Production 51
      5.2.2 Gamma-ray Production 56
      5.2.3 Conclusions 57

6. CHARACTERIZATION OF $^{2}H(d,n)^{3}He$ REACTION ON GASEOUS TARGET 58
   6.1 Cooled Windowed Deuterium Gas Target 59
      6.1.1 Target Design 59
      6.1.2 Neutron and Gamma-ray Production 64
      6.1.3 Conclusions 67
   6.2 Differentially Pumped Deuterium Gas Target 69
      6.2.1 Target Design 69
      6.2.2 Neutron and Gamma-ray Production 72
      6.2.3 Conclusions 76

7. CONCLUSIONS 78

APPENDIX A: ANALYTICAL MODEL OF FAST NEUTRON RADIOGRAPHY 80

A.1 Resonant Imaging for Detection of Objects within Mineral Matrix 80

A.2 Stochastic Limit 85

A.2.1 Single Neutron Energy Mode 85

A.2.2 Dual Neutron Energy Mode 90

A.3 Image Modeling Using Discrete-Ordinates Transport Code DORT 92

A.3.1 Description of the Model 92

A.3.2 Results and Discussion 94

APPENDIX B: DESIGN OF THE ADVANCED DEVELOPMENT MODEL 97

B.1 Housing and Shielding 97

B.2 RFQ Accelerator 103

B.2.1 Characterization of Beam Energy 106

B.2.1.1 Experimental Method 106

B.2.1.2 Results and Discussion 106

B.2.2 Characterization of rf Resonant Frequency 108

B.2.2.1 Experimental Method 108

B.2.2.2 Results and Discussion 109

B.2.3 Characterization of Beam Dispersion 109

B.2.3.1 Experimental Method 109

B.2.3.2 Results and Discussion 110

B.3 Differentially Pumped Deuterium Gas Target 116

B.4 Mineral Ore Presentation System 119

B.5 Imaging Detector 119

B.6 Control System 119

APPENDIX C: EXPERIMENTAL EVALUATION 121

C.1 Elemental Composition of the Object and Mineral Matrix 121

C.2 Imaging 125

C.2.1 Experimental Method 125

C.2.1.1 Neutron Beam 125

C.2.1.2 Data Treatment 125

C.2.1.3 Geometry 126

C.2.1.4 Samples 126

C.2.2 Results 128

C.2.3 Discussion 129

REFERENCES 137

1. INTRODUCTION

The unique properties of the neutron have been used in the study of condensed matter ever since the particle was discovered by Chadwick in 1932. Because of the lack of electric charge, neutrons can penetrate through thick solid samples virtually unaffected by the atomic electron clouds. They interact directly with atomic nuclei and the strength of interactions varies significantly not only with atomic number but also with isotopic mass. The extremely wide range of energies over which neutrons can effectively interact with the nuclei results in astonishing diversity of interaction phenomena, and gives rise to a distinct field of nuclear physics called *neutron physics*.

Neutrons are unstable as free particles and can only exist in a stable form within the atomic nucleus. Therefore, the only available sources of neutrons for research and applications are based on nuclear reactions. A tremendous effort has been devoted in the past to the development of neutron sources suitable for an ever-increasing number of applications of neutron techniques in research, medicine and industry. This effort has resulted in the development of neutron sources ranging from large multi-national research facilities to compact, robust and cost effective accelerator-based sources suitable for applications in medical and industrial environments.

Many of the neutron techniques are limited by the intensity of the neutron sources and consequently much effort has been directed towards the development of large, high neutron flux facilities such as nuclear reactors or spallation sources. Although research carried out in such establishments contributes enormously to our basic scientific knowledge, it is highly unlikely that structures of comparable complexity and cost can ever be utilized routinely in the industrial or medical environment. However, the potential of a number of neutron techniques may be significantly enhanced not only by employing more intense neutron sources but also by tailoring their neutron spectra. This presents the opportunity for small, yet powerful, accelerators, such as the radio frequency quadrupole (RFQ) linear accelerators and cyclotrons, for the generation of neutron beams tailored to particular application. Such neutron sources, because of their relative simplicity, have the potential of becoming the neutron equivalent of an X-ray tube and be confidently used in industrial or medical applications.

The objective of this thesis is to develop the science and technology to establish the rapid non-destructive radiography of large objects [1-4] using accelerator-generated fast neutron beams [5-7]. Furthermore, the feasibility of tailoring neutron spectra to enhance the contrast for specific chemical component has been investigated. An additional requirement is that the technique must be suitable for application in an industrial environment, i.e. a robust design and relatively low cost is required when compared to the value added in the industrial process.

1.1 Applications of Neutron Physics

It is not the intention to give an exhaustive review of the many applications of neutron physics, but it is worthwhile to mention some of the techniques utilizing neutrons in an environment other than a specialized research laboratory. A specific focus has been maintained on fast neutron imaging techniques.

1.1.1 Bulk Material Analysis

Neutrons are very well suited to the analysis of large quantities of material in a single operation, due to their excellent penetrating properties. In the processing of materials, the elemental composition, density, moisture content and particle size are often of importance in defining control parameters and therefore have to be assessed in near real-time. A number of review articles on neutron and nuclear techniques in general, applied to bulk material analysis have been written [8-12]. There is considerable interest in using neutrons for on-line coal analysis [13,14] and down-hole logging [15]. These experimental techniques include prompt gamma-ray neutron activation analysis (PGNAA) and neutron transmission. The neutron sources used are usually based on sealed radioisotopic sources such as ^{252}Cf and Am-Be as well as sealed tube neutron generators.

The PGNAA-based coal gauge developed at CSIRO, Australia, enables a rapid direct determination of carbon, total hydrogen, chlorine and ash content. The moisture, specific energy and Na_2O / ash values are derived from these measurements [13]. Many similar devices are operational worldwide.

Nuclear logging is well established in the oil, gas and uranium industries. The main interest in oil and gas exploration is to locate porous zones which may contain hydrocarbons and are free of clay minerals preventing the flow of fluid. The spatial distribution of thermal and epithermal neutrons resulting from interactions of high energy neutrons with the medium can be related to its hydrogen content and hence its porosity [11].

Borsaru has reviewed applications of neutron techniques for the determination of manganese grade in manganese ore, the evaluation of phosphate deposits and grade logging of bauxite deposits [15].

Selective fast neutron activation analysis via the production of nuclear isomers was used for the determination of gold in silicates [16-18]. This technique holds promise for application on an industrial scale if a suitable neutron source is developed.

1.1.2 Detection of Chemical Compounds

As opposed to quantitative elemental bulk material analysis, the aim of a substance detector is to non-intrusively identify the presence of an object containing a specified chemical compound within a specimen probed. The prime application of neutron-based substance detecting systems is the non-intrusive inspection of luggage, trucks, shipping containers, etc. for illicit materials such as explosives, drugs or certain chemicals. The development of neutron techniques for this purpose was significantly accelerated after the tragedy over Lockerbie in 1989. A review of these techniques can be found in [19-21].

Neutron beams offer the possibility of the rapid examination of large objects and they possess the elemental sensitivity required for successful detection. For the vast majority of these techniques the principle of detection is based on the correlation between O, N and C concentrations, specific and sufficiently unique, for the above mentioned substances. Depending on the specific technique, thermal or fast neutron beams are used with mono-energetic or white neutron spectra. The detection is achieved through the measurements of gamma rays resulting from neutron capture or scattering or via measurements of time-correlated neutron transmission. The neutron sources used are almost exclusively accelerator-based, in some cases requiring operation in micro-second or even nano-second pulsed mode. Each of the techniques has its specific merits and limitations and some of them are being considered for deployment.

1.1.3 Medical Applications

Neutron therapy for cancer treatment has been used in clinical practice for several decades. A promising cancer treatment, namely boron neutron capture therapy (BNCT) has recently undergone a revival and is currently under intense investigation in a number of research centers worldwide. The concept of BNCT is to load a tumor region with the ^{10}B isotope and subsequently irradiate it with keV neutrons. The neutrons, moderated in the tissue, are captured in the $^{10}B(n,\alpha)^{7}Li$ reaction. The resulting α-particle and ^{7}Li-ion carry collectively more than 2 MeV of kinetic energy which, when dissipated within the malignant cell, selectively damages it. With sufficient concentration of ^{10}B and suitable neutron flux, a substantially higher radiation dose is delivered to the tumor than to the surrounding healthy tissue. BNCT usually employs a neutron beam from a nuclear reactor or high energy particle accelerator, but recently, dedicated facilities have been considered that are based on relatively small but powerful particle accelerators with suitable moderation systems [22,23].

1.1.4 Imaging

Imaging with neutrons was pioneered by Kallman and Kuhn in 1935-1944 [24] but it is still a relatively novel technique of non-destructive examination. Radioisotope neutron sources, have for long been considered very attractive because of their portability and relative ease of use, but suffer from the shortcoming that they deliver insufficient neutron fluxes, which results in unacceptably long exposure times, and often have inconvenient half-lives. The availability of intense thermal neutron beams from nuclear reactors, which produce acceptable neutron flux, have made neutron radiography techniques possible. Yet for long it remained more a scientific curiosity than a widely accepted tool of non-destructive analysis. Neutron radiography was first used in the mid 1960's within the Apollo space program for routine inspections. Since then the number of applications of thermal neutron radiography has grown rapidly and the technique is presently a standard tool in the examination of aerospace and military aircraft, nuclear fuel, ceramic components and explosive devices. World Neutron Radiography Conferences have been held regularly since 1981 and their proceedings are excellent reviews of current research and development in the field [25-29]. With the introduction of electronic imaging detectors, such as charge coupled devices (CCD) and amorphous silicon (A-Si) plates, digital radiography and fully 3-dimensional thermal neutron tomography have become possible and are now offered as non-destructive analysis techniques at many reactor facilities.

Imaging with fast neutrons is far less mature than standard thermal neutron radiography, not to mention X-ray or gamma-ray imaging. Its inherent sensitivity is much lower than that of thermal neutron radiography, even in favorable cases. There are difficulties associated with the detection of fast neutrons in the image format and the lack of portable fast neutron sources appears to put fast neutron imaging at a disadvantage compared to the other imaging techniques. However, with the availability in the recent years of compact cyclotrons or linear accelerators capable of producing fast neutron beams from nuclear reactions in suitable target materials, some specific advantages of lower MeV fast neutron beams for imaging merit further attention.

For neutrons with kinetic energies in the MeV range, the main modes of interaction with matter are elastic and inelastic scattering. The total cross-section for most elements tends to decrease with increasing neutron energy, becoming similar for most materials at higher energies. As a result, samples are more transparent to fast neutrons facilitating the examination of larger objects. Furthermore, it is possible to exploit the resonance structure of the total cross-section function, notably for carbon, oxygen and nitrogen, in order to enhance detection. If a neutron spectrum from an accelerator-based fast neutron source can be tailored to suit a particular application by the selection of a suitable nuclear reaction and projectile energy, then images of the distribution of an element of interest can be obtained at least in principle.

Fast neutron beams are delivered directly, with no losses in the moderation process and the emitted spectrum for a given nuclear reaction can be controlled, to a degree, by the energy of the projectile. The

emission of the neutron beam takes place only when the accelerator is energized, and as such, radiation safety requirements are far simpler in comparison with the operation of a nuclear reactor, or even an intense isotopic source.

Fast neutron beams have proved to be useful in some special applications in medical radiography like the observation of changes in tumor size as a function of radiation exposure [30] or imaging air cavities behind the bone [31]. However, the high content of hydrogen in the human body results in large doses being absorbed by the patient, limiting the practical usefulness of fast neutron radiography in this area.

The work of Overley [32-34] in 1983 demonstrated that fast neutron computed tomography in conjunction with the time-of-flight technique can successfully be applied to elemental sensitive imaging. In this case fast neutron beams were produced by the bombardment of a beryllium target with 4.27 MeV deuterons obtained from a pulsed (0.5 MHz) 5 MV Van de Graaff accelerator. A proton-recoil scintillation detector was used for neutron detection. Although, for biological samples, the sensitivity and spatial resolution of neutron imaging was considerably lower than for X-ray imaging, the high penetrating power of the neutron beam and its elemental sensitivity were recognized as potential advantages, off-setting these disadvantages.

Duhmke *et al.* [35] used fission neutrons to produce radiographic images of large hydrogen-containing objects, which could not be examined with thermal neutrons due to insufficient transmission. They have also performed fast neutron radiography on live humans during fast neutron radiotherapy, using a sealed D-T tube [36]. Tumors hidden in X-ray imaging were clearly identifiable in most of these fast neutron radiographs. In both cases track-etch detectors were used for neutron image registration.

High quality fast neutron tomographic images of laboratory samples and various technical objects were produced by a research group in Stuttgart, Germany [37-39]. They utilized a narrow single beam of reactor fission neutrons to scan the object with a liquid organic scintillator for detection. The disadvantage of a single beam technique is that the image acquisition time is excessive (i.e. well in excess of 5 hours) but the image quality can be improved significantly by separation of the gamma-ray component, by using pulse shape discrimination technique. This results in the simultaneous acquisition of separate neutron and gamma-ray images as well as the combined image. A spatial resolution of 0.1 mm and a density resolution better than 2 % was demonstrated in the use of the Stuttgart group's fast neutron tomography system. The fast neutron imaging is mostly used for localization of hydrogen containing materials, such as plastic and water, in the presence of high density metals.

The feasibility of neutron imaging for drug and explosive detection has also been studied [40-42]. It was demonstrated that energy dependent neutron attenuation can in principle be used for the detection of key elements, such as N, O and C. The simple determination of areal densities is not sufficient for identification and full tomographic reconstruction is too time consuming, a real-time neutron laminography has been proposed [43]. Theoretical studies indicate that such techniques may meet the required detection rate and reliability requirements.

In spite of a number of fast neutron imaging techniques being researched and developed, there is little information available on industrial applications. A number of techniques utilize nuclear reactor-based neutron sources, which clearly put them at a disadvantage when industrial applications are concerned. The technical complexity of others means that further testing and verification in the laboratory must be undertaken before they reach the necessary maturity, reliability and robustness for industrial applications. Clearly, the success of fast neutron imaging techniques outside a controlled laboratory environment depends on the development of portable, powerful and robust accelerator-based neutron sources.

1.2 Outline of This Thesis

The objective of this project is to investigate the detailed physics of neutron production and interactions in order to develop an effective solution allowing for the rapid non-destructive examination of large objects using fast neutron radiography. The technique under investigation is to be capable of the visualization of the internal structure of particular samples and the detection of a substance or object of interest. A unique aspect of this work is the specific detection or isolation of particular substances or species by the use of a dual energy resonant imaging technique.

The objective is to be achieved by research into the following areas:

1. characterization of fast neutron sources at low incident particle energies ($E \leq 10$ MeV);
2. modeling of the neutron transport and image formation in the imaging detector;
3. development of an experimental set-up demonstrating the capability of the technique.

The methodology being developed is to be verified experimentally in applications in mineral identification and elemental imaging for the detection of hidden chemical substances. Resonant fast neutron imaging may potentially be used in an industrial processes in mining and mineral processing for effective sorting of mineral ores.

An additional requirement imposed on the technique is that it will be installed in an industrial environment so the neutron generator employed for this application has to be compact and robust. The suitability of commercially available small accelerator technologies has been reviewed considering the requirements placed on the accelerator by the detection technique, and in the light of the physics of neutron production.

The material in this thesis is presented in 7 chapters:

- chapter 1 introduces the applications of the neutron physics;
- chapter 2 gives a brief review of the neutron sources used in research and applications with a specific focus on the accelerator-based neutron sources;

- chapter 3 describes the experimental methods used in the course of this project;
- chapter 4 presents the results obtained by the time-of-flight technique for the characterization of the 'white' neutron spectrum reactions: $^{9}Be(d,n)^{10}B$ and $^{7}Li(d,n)^{8}Be$;
- chapter 5 presents the results obtained by the time-of-flight technique for the characterization of the quasi mono-energetic neutron spectrum reactions: $^{9}Be(p,n)^{9}B$ and $^{7}Li(p,n)^{7}Be$;
- chapter 6 presents the results of the time-of-flight characterization of the $^{2}H(d,n)^{3}He$ reaction on the gaseous targets;
- chapter 7 concludes this thesis with a brief discussion of the directions of the future research;
- appendix A examines the stochastic limits of fast neutron radiography imposed by the Poisson statistics and presents the results of modeling of neutron and gamma-ray imaging, based on discrete-ordinates radiation transport codes; the model was developed in co-operation with Dr G. Pfister from Institut für Kernenergetik und Energiesysteme (IKE), University of Stuttgart, Germany;
- appendix B discusses the design and characterization of the advanced development model (ADM) for industrial application of fast neutron radiography for detection of objects within mineral matrix.; the author is a member of a larger project team responsible for the development of the ADM, in charge for the physics aspects of the design (radiological protection, development of technical specification and characterization of the accelerator, gas target and detector, experimental geometry),
- appendix C presents the experimental evaluation of the ADM.

2. NEUTRON SOURCES

A number of criteria, such as intensity, spectral distribution and method of generation, can be used in the classification of neutron sources. The last of these criteria has been used in this thesis. Specific attention is focussed on accelerator-based neutron sources as these are believed to be best suited to many industrial applications.

2.1 Radioisotopes

The main advantages of sealed radioisotope neutron sources are their small size, low cost and comparative ease of maintenance. The neutron yield of these sources is directly proportional to the amount of material used and its rate of decay. The limitations are: short half-lives, broad neutron spectrum and the presence of significant amount of other types of radiation (mainly gamma-rays) accompanying the neutrons.

The most commonly used radioisotopic neutron source is based on ^{252}Cf, which produces neutrons in a spontaneous fission process. It has a convenient half-life of 2.65 years and produces 2.34×10^{12} neutrons per second per gram. It emits neutrons in a wide energy band stretching from above zero to above 12 MeV, with a mean energy of 2.14 MeV.

Most of other radioisotopic neutron sources of practical significance are based on the (α,n) nuclear reaction. They consist of an α-particle emitting isotope, such as ^{239}Pu or ^{241}Am, mixed with target material, usually Be. Although half-lives, yields and spectral shapes depend on the specific type of the source used, they are, to a large extent, comparable with ^{252}Cf.

The use of radioisotope neutron sources is of limited value in applications where high intensities and well-defined neutron energy bands are required. The detail characteristics of radioisotope neutron sources can be found in several references, e.g. [44].

2.2 Nuclear Reactors

Nuclear fission reactors are commonly used as neutron sources for research purposes. They are capable of producing by far the highest fluxes of neutrons.

Neutrons produced in a reactor have a considerable range of energies. Fission neutrons can have energy only slightly above thermal energy (0.025 eV) to more than 10 MeV. Therefore, precise analytical techniques requiring well-defined energy and energy band cannot use the fission neutrons directly and

require moderation or some means of sorting of the neutrons by energy. This results in a significant reduction of the available neutron flux and often makes accelerator-based neutron sources more viable for particular applications.

Nuclear reactors are generally too large and expensive to be useful in industrial applications. An additional disadvantage is that the source cannot easily be switched off and requires continuous operation with expensive and often cumbersome radiation protection measures. Although research reactors are clearly different from reactors used in the nuclear power stations, following a number of much publicized accidents, there is growing public resistance to the construction of new units.

2.3 Accelerator-based Sources

Neutrons can be produced in nuclear reactions induced by charged particle beams from accelerators. In such reactions compound nuclei are usually formed, which are excited with a sum of the binding energy and the kinetic energy of the projectiles. If this excitation energy is larger than the binding energy of the last neutron in the resulting compound nucleus then there is high probability of neutron emission. The balance of the excitation energy is distributed as kinetic energy between the neutron and residual nucleus and the excitation energy of the residual nucleus, which returns to its ground state by gamma-ray emission. On the other hand, some neutron-producing reactions proceed directly, without the formation of a compound nucleus, as observed in deuteron stripping reaction.

The target materials are usually pure elements or chemical compounds in the solid state. Gaseous targets have sometimes been used if reactions between hydrogen isotopes are of interest.

The most commonly used neutron producing reactions are (d,n) and (p,n) nuclear reactions. In the (d,n) reactions a very highly excited compound nucleus is formed following a deuteron capture due to its small binding energy. Consequently, nearly all (d,n) reactions are exothermic. All (p,n) reactions on stable nuclei are endothermic with a threshold energy of at least 0.782 MeV (Q-value of a β–decay of the neutron).

The nuclear reactions resulting in the emission of neutrons with mono-energetic or quasi mono-energetic spectra are of particular importance for many applied neutron techniques. Generally, a neutron beam is regarded as mono-energetic if the neutron energy spread is small in comparison with the energy itself. Only accelerator-based sources are capable of producing significant fluxes of mono-energetic neutrons. As the ion beam traversing a target material rapidly loses its kinetic energy, 'thin' targets must be used for the generation of mono-energetic neutrons. The broadening of the neutron energy spectrum can be controlled by the target thickness and eventually, for 'thick' targets, i.e. the targets of thickness sufficient for complete stopping of the incident beam, the resulting neutron spectrum covers the full range from the maximum energy down to zero. There is clearly a trade-off between the neutron flux (a maximum for thick targets)

and well defined neutron energy (best for thin targets) which has to be considered for each specific application.

Mono-energetic neutrons with high intensities are most commonly produced by the 'big four' reactions listed in Table 1.

Reaction	Q-value [MeV]	Break-up Reaction	Break-up threshold [MeV]	Mono-energetic neutron energy range [MeV]
$^{2}H(d,n)^{3}He$	+ 3.270	D(d,np)D	4.45	1.65 – 7.75
$^{3}H(d,n)^{4}He$	+ 17.590	T(d,np)T $T(d,2n)^{3}He$	3.71 4.92	11.75 – 20.5
$^{3}H(p,n)^{3}He$	- 0.763	T(p,np)D	8.35	0.3 - 7.6
$^{7}Li(p,n)^{7}Be$	- 1.644	$^{7}Li(p,n)^{7}Be^{*}$	2.37	0.12 – 0.6

Table 1. Data of the 'big four' mono-energetic neutron source reactions [45].

In addition to the traditionally used mono-energetic neutron reactions listed in Table 1, the inverted (p,n) reactions have recently received considerable attention as potential intense sources of mono-energetic neutrons [46]. In such reactions: $^{1}H(t,n)^{3}He$, $^{1}H(^{7}Li,n)^{7}Be$, $^{1}H(^{11}B,n)^{11}C$ and $^{1}H(^{13}C,n)^{13}N$, the projectile is heavier than the target, which results in kinematically collimated neutron beams. The main advantages of such neutron sources are high neutron output and the confinement of neutrons into a forward cone. The disadvantage is that a considerably higher projectile energy is required.

White neutron sources (broad continuous energy spectra described as 'white' using an optical analogy) are used in applications where the neutron energy is of secondary importance. At lower projectile energies nuclear reactions such as: $^{9}Be(p,n)^{9}B$, $^{9}Be(d,n)^{10}B$, $^{12}C(d,n)^{13}N$ or $^{7}Li(d,n)^{8}Be$ are commonly used.

Bombardment of heavy mass nuclei with projectiles in the 20 – 100 MeV energy range results in an evaporation or Maxwellian neutron spectrum, in most cases.

The spallation process typically occurs when the energy of the incident projectile exceeds 100 MeV. Cascades of neutrons with broad energies are emitted as a result of 'heating' of the nucleus. The intensity of neutron beams obtainable from spallation sources like the Paul Scherer Institute's SINQ [47] are comparable with these generated by nuclear reactors.

The intensity of neutron beams generated by accelerator-based neutron sources in a particular nuclear reaction depends on the target current. The cross-sections for neutron production are typically of the order of tens to hundreds of milli-barns, and vary significantly with projectile energy. Large charged particle currents, of the order of tens or hundreds of micro-amperes, or even of the order of milli-amperes, need to be accelerated in order to produce the neutron fluxes required for industrial and other applications, with outputs typically in excess of 10^{11} neutrons per second into 4π. The privilege of working with such intense neutron beams was for long reserved for large research establishments operating expensive and complex high power accelerators. For practical reasons such accelerators could not be used in industrial or medical environment on a large scale.

Sealed tubes utilizing the $T(d,n)^4He$ and $D(d,n)^3He$ reactions were the only accessible neutron generators capable of delivering a neutron flux with an intensity sufficient for most of practical applications. Although meeting neutron flux requirements, sealed tube neutron generators have a number of serious limitations. The most important is a considerable fall of the neutron yield with time and limited lifetime of the tube due to deterioration of the target. The longest lived tubes reached only 500 hours with significant deuterium build-up in the target and hence a neutron yield decrease [48]. The used tubes had to be replaced at significant cost.

The development of relatvely compact, inexpensive and powerful accelerators such as RFQ linacs [49] or cyclotrons [50], has enabled research on applied neutron techniques at reasonable cost. Such accelerators operate at low energy, usually below 10 MeV, and can be used with a variety of targets. They are relatively lightweight, rugged and have an easy to maintain modular structure. The units are usually self-contained, with closed circuit cooling systems and low power consumption for increased portability. The maximum particle beam currents range from 100 μA to above 1 mA, which translates to neutron outputs well in excess of 10^{12} neutrons per second, depending on the target employed. High current capability and flexibility of accelerated particles and output energies make these modern accelerators well suited to provide neutron fields for a variety of applications. Technical specifications of selected commercially available accelerators are presented in Table 2.

The technique being developed requires high flux of mono-energetic neutrons so clearly an accelerator-based neutron source is required. Additional requirements for industrial applications make small commercially available accelerators an ideal choice. Such accelerators are capable of producing intense neutron beams at a low incident particle energy. Therefore, the detailed characteristics of a practical set of neutron producing nuclear reactions needed to be investigated for the successful application of this technology.

In spite of the considerable literature on the subject, there is still a need for the detailed characterization of accelerator-based neutron sources. A significant portion of the current knowledge on neutron-producing nuclear reactions is based on experimental work conducted in 1950's and 1960's. The focus of most of those experiments was to establish the reaction mechanism and to investigate the energy level structure of the residual nucleus.

Model	Company	Type of Accelerator	Incident Particle	Beam energy [MeV]	Maximum beam current [μA]	Neutron Yield [n s^{-1}]
TN 46	Sodern, France	(D,T) Tube	D	0.225	10000	4×10^{11}
DL-1.5	AccSys, USA	RFQ Linac	D	1.5	325	1×10^{11}
PL-4	AccSys, USA	RFQ Linac	P	3.9	1000	1.3×10^{12}
Cyclone 3D	IBA, Belgium	Cyclotron	D	3.8	2000	5.7×10^{12}
Cyclone 18+	IBA, Belgium	Cyclotron	P	18	2000	2.1×10^{14}

Table 2. Typical specification for selected commercially available accelerators used as neutron generators. The neutron outputs have been calculated for cyclotrons and RFQ linacs utilizing a beryllium target. Data compiled from references [49,50].

Therefore, thin targets were usually used and limited time-of-flight spectra were reported. Many important details of the characteristics were left out or were discussed only qualitatively. Moreover, the energy range covered in these experiments was often higher than that of interest for the present work and the extrapolation of these results was not always possible. This thesis therefore, present new data on the selected nuclear reactions with a specific focus on their application in fast neutron radiography with commercially available accelerators.

The set of neutron-producing nuclear reactions, for the purpose of this thesis, was based on three criteria: neutron yield, the physical characteristics of the target material and possibilities for mono-energetic neutron production. The following nuclear reactions were investigated:

1. white neutron sources: $^9Be(d,n)^{10}B$, $^7Li(d,n)^8Be$ and $^9Be(p,n)^9B$;
2. mono-energetic or quasi mono-energetic neutron sources: $^2H(d,n)^3He$, $^7Li(p,n)^7Be$ and $^9Be(p,n)^9B$.

It was decided from the outset of this work that for safety reasons the nuclear reactions involving tritium would not be investigated. The incident particle energies used in investigations of specific nuclear reactions are listed in Table 3.

Since the review articles of Brolley and Fowler [51], in 1958, which covers, at least qualitatively, most of the current knowledge on the mono-energetic neutron properties, there have been several review articles published [46, 52-54].

Nuclear reaction	Incident beam energy [MeV]
^{9}Be(d,n)^{10}B	0.9; 1.5; 4.0
^{7}Li(d,n)^{8}Be	0.9; 1.5; 4.0
^{9}Be(p,n)^{9}B	3.0 – 9.95*, 2.57; 3.0; 4.0
^{2}H(d,n)^{3}He	2.1*; 5.0*
^{7}Li(p,n)^{7}Be	2.36*; 3.7*; 2.32; 4.28

Table 3. A selection of neutron producing nuclear reactions investigated in this thesis with incident particle energy. *Only TOF spectra are presented.

A very comprehensive review of the mono-energetic neutron production was given by Drosg and Schwerer [55] and covered the angular dependence of neutron energies and cross-sections for neutron production for the following nuclear reactions: ^{1}H(t,n)^{3}He, ^{1}H(^{7}Li,n)^{7}Be, ^{2}H(d,n)^{3}He, ^{2}H(t,n)^{4}He, ^{3}H(p,n)^{3}He, ^{3}H(d,n)^{4}He and ^{7}Li(p,n)^{7}Be.

There are few publications covering the less commonly used fast neutron producing reactions, for projectile energies lower than 10 MeV. Neutron yield and spectra from proton bombardment of ^{6}Li, ^{7}Li, ^{9}Be, ^{11}B, and ^{18}O can be found in [56], while Drosg reviewed ^{9}Be(p,n)^{9}B, ^{11}B(p,n)^{11}C, ^{51}V(p,n)^{51}Cr and ^{9}Be(α,n)^{12}C reactions [57]. Grand and Goland [58] discussed the Serber's deuteron stripping reaction theory applied to the ^{7}Li(d,n)^{8}Be and ^{9}Be(d,n)^{10}B reactions and the comparative characteristics of neutrons from these reactions were discussed in [59,60].

Due to its high neutron yield and good thermal properties of metallic Be targets the ^{9}Be(d,n)^{10}B reaction is relatively well studied at projectile energies below 10 MeV [61-67].

The renewed interest in the reaction ^{9}Be(p,n)^{9}B as a source of neutrons for cancer treatment by BNCT has resulted in more detailed studies of this reaction at low incident proton energies [68-70].

The most recent review of the neutron producing reactions for neutron energies between 20 keV and 200 MeV was carried out by Drosg [71,72], with special emphasis on new developments at low and high energies, sources of kinematically collimated neutrons and intense mono-energetic neutron sources.

Although most of the detectors used with neutron techniques are sensitive to gamma-rays, there is little information in the literature concerning gamma-ray emission accompanying neutron production. This is necessary both for radiographic and medical uses of neutron sources. The gamma-ray intensities and spectra have to be measured in order to assess their influence on the detection process. This is particularly important for imaging techniques where an excessive amount of gamma-rays may significantly decrease expected neutron contrast.

3. EXPERIMENTAL METHOD

This chapter details the experimental techniques used for characterization of the neutron reactions and in the determination of the performance parameters of the linear accelerator used in this project. The modeling techniques and experimental specimens are also described here.

3.1 Time-of-flight Technique

The time-of-flight (TOF) technique was applied to the measurements of neutron and gamma-ray spectra, for selected nuclear reactions. In this technique the neutron energy is determined from the measurement of its velocity. The problem is to measure the time elapsed for a neutron originating in the source to reach a detector. The solution requires that the time of origin of a neutron be localized by producing neutron bursts of short (~ ns) but well-defined duration and appropriate repetition rate (~ MHz for MeV neutrons). In the investigation of accelerator-based nuclear reactions this is achieved by producing pulsed ion beams with one of several techniques such as plasma pulsing and beam chopping or bunching. The finite size of a bunch, the length of the neutron flight path, the detector dimensions and the rise time of the electronics, all contribute to finite timing resolution of the technique and limit the neutron energy resolution that is achievable. The details and theory of the time-of-flight technique is described by Neiler and Good [73], and others.

The experiments were performed at the South African National Accelerator Centre (NAC) using a 6 MV Van de Graaff accelerator. The 2 ns pulses of deuterons or protons, with a 2 MHz repetition rate, were produced by means of the time-of-flight chopper and a double gap buncher [74]. The beam current was usually kept below 1 μA, in order to reduce the detector dead time. Various targets were mounted at the end of the beam-line, positioned in the center of a large experimental hall to minimise the effects of scatter. Targets were electrically insulated from the rest of the beam-line, allowing the measurements of the beam current. The timing signal for the TOF measurements was generated by a capacitative beam pick-up system installed near the target.

A cylindrical 5 x 2.5 cm (thick) NE102a plastic scintillator [75] coupled to a fast photo-multiplier tube served as the TOF neutron and photon detector. A 200 cm^3 intrinsic germanium detector manufactured by Detector Systems GmbH (DSG), Germany [76] was used as the gamma-ray detector. The detectors were positioned at distances of 1 to 5 m from the target. Additionally, the TOF detector was mounted on a swiveling tower, which enabled easy acquisition of spectra at different laboratory angles, in the range 0° - 140°. Unless stated otherwise, the gamma-ray detector was positioned at 40° relative to the beam-line.

The conventional TOF technique was used for measurements of neutron spectra with the plastic scintillator detector. The TOF spectra to high purity germanium detector were simultaneously recorded and gamma-ray spectra gated with the duration of the gamma-ray peak in the TOF spectrum were also measured. These TOF-gated gamma-ray spectra represented the true gamma-ray emission from the target and the target area, during a beam pulse. A block diagram of the electronics and data acquisition system is presented in Figure 1.

3.2 Response and Efficiency of the Detectors

The quality of a neutron spectrum measurement with the TOF technique depends on the knowledge of the detection efficiency as a function of neutron energy. The efficiency of a proton recoil detector, such as a plastic scintillator, is also a function of the pulse height bias, which is applied in order to discriminate against the inherent photo-multiplier tube noise. The plastic scintillator detector used in these experiments was biased to approximately 250 keV of the recoil proton energy, by using a discriminator level set to approximately 1/20 of the energy of Compton edge for ^{137}Cs 662 keV gamma-ray (E_C = 478 keV). The detection efficiency function was determined by comparison of the yields of angular distribution measurements with corresponding differential cross-sections for the mono-energetic neutrons producing reactions: $^{7}Li(p,n)^{7}Be$ and $^{2}H(d,n)^{3}He$, using data from Liskien and Paulsen [77,78]. The measured neutron detection efficiency function for the detector specified above is presented in Figure 2.

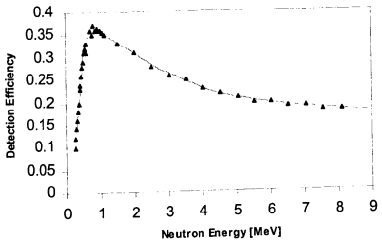


Figure 2. The experimental neutron detection efficiency for the plastic scintillator used in this work. The detector was biased at ~ 250 keV of proton recoil energy. Moving average 2-point best fit line is superimposed on a set of experimental data points.

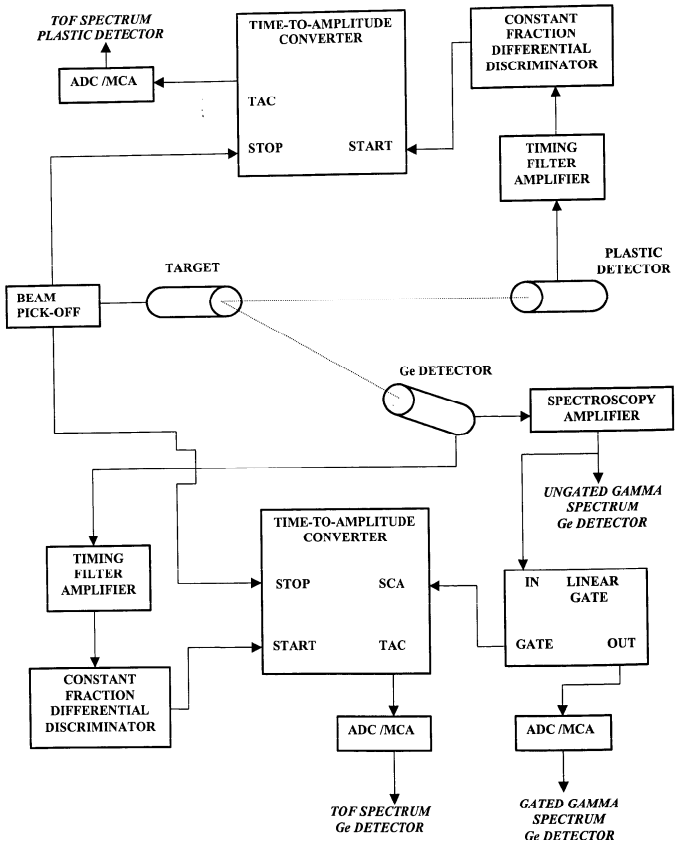


Figure 1. Block diagram of electronics set-up used in time-of-flight experiments.

The set of experimental data points is limited to a range of neutron energies from above the bias energy to about 8 MeV, in the case of the reaction $D(d,n)^3He$, due to the maximum achievable terminal voltage of 5.5 MV for the accelerator used. Although this neutron energy range is sufficient for the investigation of most of the neutron spectra relevant to this thesis, it was necessary to extrapolate the efficiency function to ~ 20 MeV, for use with the highly exoergic $^7Li(d,n)^8Be$ reaction. The portion of the efficiency curve between 8 MeV and 20 MeV was therefore linearly extrapolated from experimental data

The gamma-ray detection efficiency of the intrinsic germanium detector was determined using a calibrated ^{152}Eu source. This source enabled calibration in the gamma-ray energy range of 244.7 to 1408 keV. A straight line was subsequently fitted to the experimental data on a log-log scale, using a linear regression method. The best-fit equation, for the above energy range was:

$$D_{eff} = 5884.05 \cdot E_{\gamma}^{-0.764}, \quad (1)$$

where: D_{eff} is the detection efficiency and E_{γ} is the gamma-ray energy. This formula was subsequently used for the correction of gamma-ray energy spectra in the full acquisition range of 0-8191 keV. The experimental gamma-ray detection efficiency for the DSG intrinsic germanium detector is presented in Figure 3, for the gamma-ray energy range of 244.7 – 8191 keV.

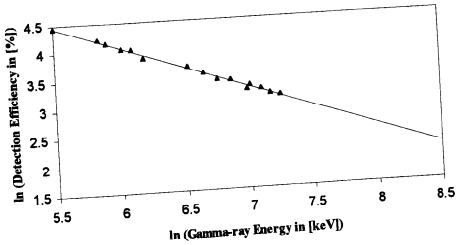


Figure 3. The experimental gamma-ray detection efficiency, over the 244.7 – 8191 keV energy range, for the DSG intrinsic germanium detector used in this work. The best fit linear regression is superimposed on the set of experimental data.

3.3 Data Treatment

The time-uncorrelated background was subtracted from all TOF spectra. The spectra were then corrected for the detector's dead-time and experimental geometry and normalized to the integrated charge of the incident beam. The TOF spectra were transformed into neutron energy spectra using the non-relativistic relation:

$$E_n = \frac{1}{2} \cdot m_n \cdot \frac{s^2}{t^2}, \qquad (2)$$

The equivalent energy width of each channel is then:

$$\Delta E_n = m_n \cdot s^2 \cdot \frac{\Delta t}{t^3}, \qquad (3)$$

where: E_n is the neutron energy, m_n is the neutron mass, s is the neutron flight path, t is the neutron flight time, ΔE_n is the neutron energy resolution and Δt is the timing calibration, i.e. the width of a channel in the TOF spectrum. The timing resolution of the TOF set-up was determined by measurement of full-width-half maximum (FWHM) of the gamma-ray peak in the TOF spectrum. It was usually of the order of 2 ns. It can be seen, by combining equations (2) and (3), that the neutron energy resolution, ΔE_n, is proportional to $E_n^{3/2}$ and therefore the best absolute resolutions are obtained at low neutron energies, for a constant flight path. For example, for a flight path of 2 m and a timing resolution of 2 ns, energy resolution at neutron energy of 8 MeV is ~ 500 keV as opposed to only ~ 8 keV at neutron energy of 0.5 MeV. With a constant timing resolution, for the transformation into neutron energy spectra, the TOF spectra are compressed in the long TOF region and expanded in the short TOF region. The absolute neutron yield is presented with respect to a solid angle of 1 sr and an integrated beam current of 1 μC. The low neutron energy cut-off present in all spectra is due to detector bias.

The laboratory gamma-ray background spectra acquired under the same experimental conditions were subtracted from all the gamma-ray spectra. The spectra were corrected for the detector dead-time and experimental geometry. The gamma-ray energy calibration was 1 keV per channel, usually 8k channels were collected. The gamma-ray energy spectra displayed in this thesis, for example in Figure 10, were not corrected for detection efficiency and are scaled in counts sr^{-1} μC^{-1}, for convenient comparison. The correction for detection efficiency was carried out where quantitative information such as gamma-ray yields or intensities of particular gamma-ray lines were discussed. The units used for gamma-ray photons are sr^{-1} μC^{-1}. The low gamma-ray energy cut-off present in all spectra is due to a preset discrimination level.

4. CHARCTERIZATION OF THE ^{9}Be(d,n)^{10}B AND ^{7}Li(d,n)^{8}Be REACTIONS

4.1 ^{9}Be(d,n)^{10}B

The ^{9}Be(d,n)^{10}B reaction with several MeV deuterons incident on a thick Be target is particularly favored for applications such as activation analysis, radiography, nuclear waste assay or radiotherapy. The reaction is very prolific, with possibly only ^{7}Li(d,n)^{8}B matching its yield, for charged particle energies below 10 MeV. The metallic Be used for target construction can be easily machined and is capable of tolerating beam currents in excess of 100 μA with a straightforward target design and cooling. The reaction is exothermic with a positive Q-value of 4.36 MeV, which results in a neutron spectrum extending to quite high energies. The lower energy neutron yield may be complicated by a number of multi-body reactions (Table 4).

Reaction	Q-value [MeV]
^{9}Be(d,n)^{10}B	+ 4.36
^{9}Be(d,^{4}He)^{7}Li	- 1.10
^{9}Be(d,pn)^{9}B	- 2.20
^{9}Be(d,p2n)^{4}He	- 3.80

Table 4. Nuclear reactions contributing to neutron production in bombardment of ^{9}Be with low energy deuterons.

Neutron energy spectra and yields for the Be(d,n) reaction have been previously reported by several authors, mostly in the higher deuteron energy range [59-67, 79]. The main characteristics of this reaction have been established but important details still have to be determined. The available data for deuteron energies E_d < 4.0 MeV is very fragmented. Hence, the Be(d,n) reaction was studied systematically at incident deuteron energies of 0.9, 1.5 and 4.0 MeV. These energies were chosen to correspond to the incident deuteron energies of standard RFQ linacs, commercially available from AccSys Technology [49].

4.1.1 Neutron Production

Typical TOF spectra for a deuteron of energy E_d = 4.0 MeV incident on 2 mm and 5 μm Be targets are presented in Figure 4. As many as 10 neutron groups corresponding to various residual states of the ^{10}B nucleus (Figure 5) were resolved in the thin target spectrum: n_o = 8.36 MeV ($^{10}B(0)$ = 0 MeV), n_1 = 7.64 MeV ($^{10}B(1)$ = 0.718 MeV), $n_{2,3}$ = 6.40 MeV ($^{10}B(2,3)$ = 1.740, 2.154 MeV), n_4 = 4.73 MeV ($^{10}B(4)$ = 3.587 MeV), n_5 = 3.49 MeV ($^{10}B(5)$ = 4.774 MeV), $n_{6,7,8}$ = 3.10 MeV ($^{10}B(6,7,8)$ = 5.11, 5.16, 5.18 MeV), $n_{9,10}$ = 2.20 MeV ($^{10}B(9,10)$ = 5.92, 6.025 MeV), n_{11} = 2.04 MeV ($^{10}B(11)$ = 6.127 MeV), n_{12} = 1.55 MeV ($^{10}B(12)$ = 6.561 MeV) and $n_{13,14}$ = 1.10 MeV ($^{10}B(13,14)$ = 6.881, 7.0 MeV) . The thick target spectrum obviously reflects the features of a thin target spectrum folded with the slowing down of the incident deuterons in the target material.

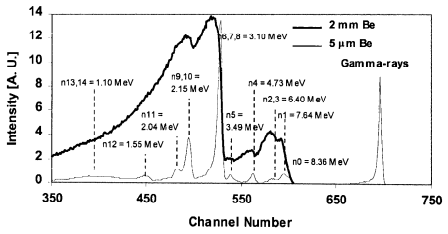


Figure 4. Time-of-flight spectra of the ^{9}Be(d,n)^{10}B reaction at incident deuteron energy of 4.0 MeV, at 0°, obtained with targets of 2 mm and 5 μm thickness. Neutron groups corresponding to different final states of the residual ^{10}B nucleus are indicated.

Figures 6a-6f show the spectral distributions from the thick target Be(d,n) reaction measured for deuteron energies of 0.9, 1.5 and 4.0 MeV , at 0° – 120° range of laboratory angles.

There is a dramatic change of spectral shape when deuteron particles are accelerated beyond 1 MeV due to the appearance of lower energy neutrons leaving ^{10}B in one or more of the final states at 5.11, 5.163 and 5.18 MeV (Figure 5) (E_n < 1 MeV and E_n < 3.5 MeV for deuteron energies of 1.5 and 4.0 MeV, respectively). These lower energy neutrons dominate the spectra and rapidly increase the yield for E_d > 1 MeV. The higher energy neutron groups correspond to transitions to the ground and the first five excited states in ^{10}B namely, 0.718, 1.740, 2.154, 3.587 and 4.774 MeV (Figure 5).

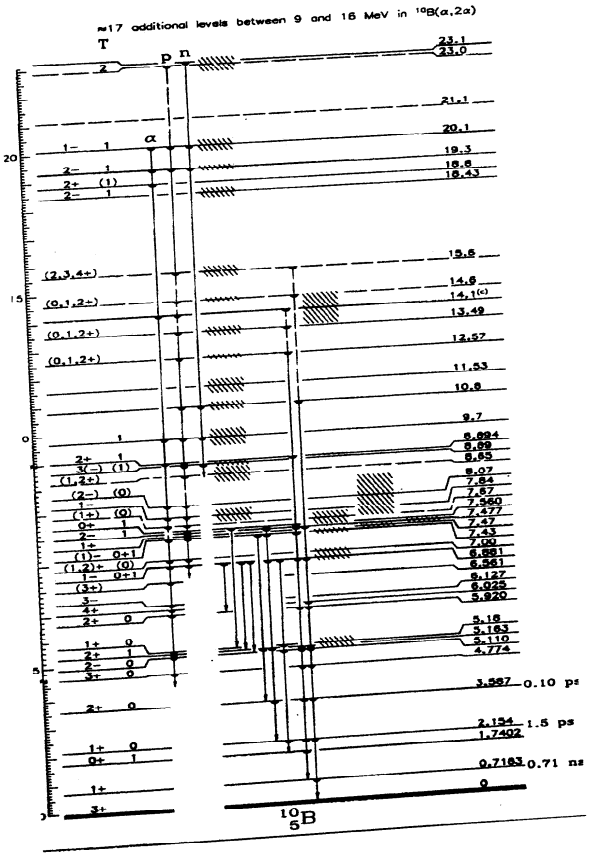


Figure 5. Nuclear level structure of ^{10}B [80].

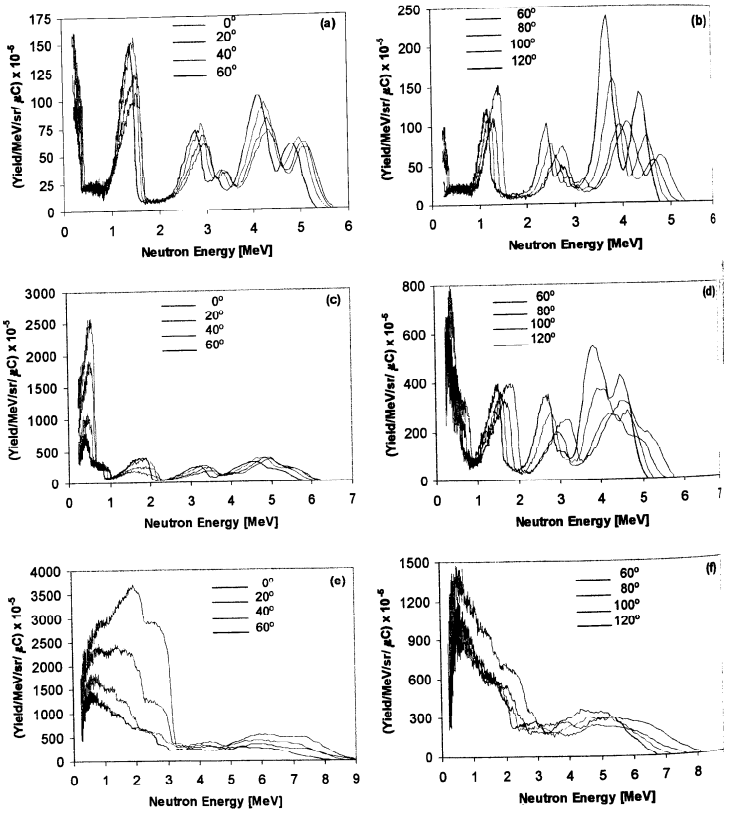


Figure 6. Neutron spectra at a range of laboratory angles of 0°–120° produced in bombardment of a thick Be target with deuterons of energy 0.9 MeV (a,b), 1.5 MeV (c,d), 4.0 MeV (e,f).

The Be(d,n) thick target yields are presented in Figures 7a-7c.

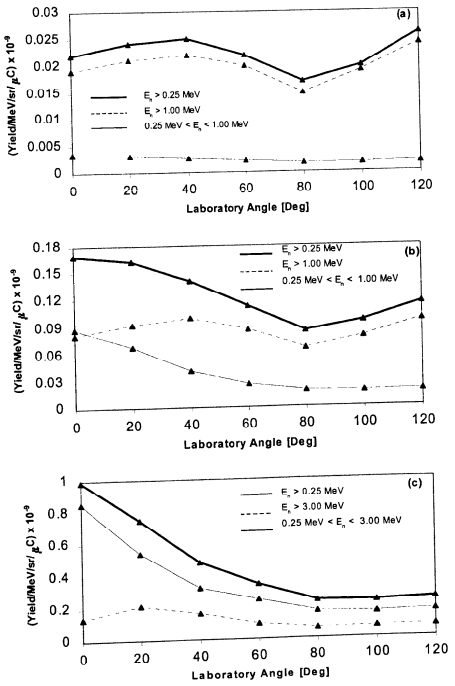


Figure 7. Neutron yield angular distributions for thick target Be(d,n) reaction at deuteron energies of 0.9 MeV (a), 1.5 MeV (b) and 4.0 MeV (c).

The common features of the angular dependence of the thick target yields can be discussed on the basis of the yield curve for E_d = 1.5 MeV (Figure 7b). The yield curve for the lower energy neutron groups has its maximum at 0° and decreases with increasing laboratory angle and does not exhibit any significant structure. The yield for the higher energy group increases initially and peaks at 20°-40°. Peaking at angles away from 0° is a characteristic feature of the (d,n) stripping process, where the proton is captured with an angular momentum of $l \geq 1$. Bauman *et al.* compared the angular distributions with a direct reaction theory using the distorted wave Born approximation (DWBA) for E_d = 8 MeV [64]. The first four transitions compared very well with DWBA and show the typical pattern of a stripping process. The structureless yield curve for the lower energy neutron groups indicates the superposition of different processes and angular momentum transfers.

The calculated average neutron energies (Figure 8) are in very good agreement with data published by Meadows [65] (Figure 9), but differ significantly from data by Inada *et al.* [61] due to their overestimation of neutron forward peaking effect, later corrected by Whittlestone [62].

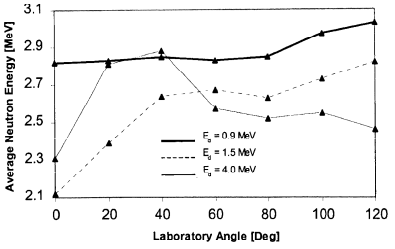


Figure 8. Average neutron energies for thick target Be(d,n) reaction spectra at deuteron energies of 0.9 MeV, 1.5 MeV and 4.0 MeV.

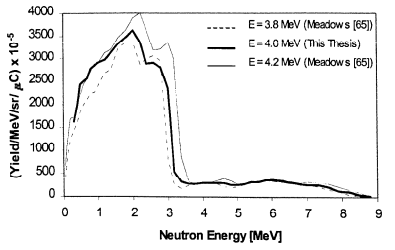


Figure 9. Comparison of spectral shapes between Meadows [65] and the present study.

4.1.2 Gamma-ray Production

A TOF-gated gamma-ray energy spectrum taken at a laboratory angle of 80°, for E_d = 4.0 MeV, is presented in Figure 10.

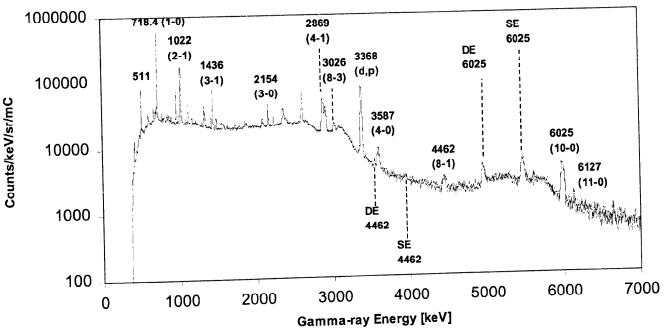


Figure 10. Thick target Be(d,n) reaction TOF-gated gamma-ray spectrum at a deuteron energy of 4.0 MeV obtained at a laboratory angle of 80°. The numbers indicate the energies of the gamma-ray lines in keV, and transitions corresponding to ^{10}B excitation levels are given in brackets; SE and DE stand for single escape and double escape, respectively and (d,p) indicates the gamma-ray lines resulting from the ^{9}Be(d,p)^{10}B reaction.

The gamma-ray spectra for all incident deuteron energies under investigation were dominated by the 718 keV emission, corresponding to transition from the first excited state to ground state in the ^{10}B nucleus. Also clearly seen were: 1022, 1436 and 2869 keV lines resulting from transitions from levels: 2 (1740 keV), 3 (2154 keV) and 4 (3587 keV) to level 1 (718.4 keV). With the exception of level 2, the transitions to the ground state were also evident and they were always significantly weaker than the transitions to the first excited level.

The 4462 keV and 3026 keV lines corresponded to transitions to level 1 and 3 from level 8 (5180 keV) These appear in the spectra for E_d = 1.5 MeV and E_d = 4.0 MeV (Figure 10). For both deuteron energies the 8-3 transition was stronger than the corresponding 8-1 transition.

Finally, the 6025 keV and 6125 keV lines, correspond to ground state transitions from levels 10 and 11, respectively, and were seen in the spectrum for E_d = 4.0 MeV. The 3368 keV gamma-ray line, resulting from a transition to the ground state from the first excited state in ^{10}B in the competing ^{9}Be(d,p)^{10}B reaction (Q = + 4.59 MeV), was pronounced in all spectra.

The relative gamma-ray intensities for transitions going from level 4 to 0 in ^{10}B are approximately 1:4:10 for E_d = 0.9 MeV, E_d = 1.5 MeV and E_d = 4.0 MeV, respectively. These correspond well to the observed relative intensities of the higher energy neutron groups that result from the stripping process. For the transitions from level 8, the relative gamma-ray intensities are approximately 1:8 for E_d = 1.5 MeV and E_d = 4.0 MeV which compares very well with the relative intensities of the relevant low energy neutron groups. It is clear from the above results that the neutron groups corresponding to excited states in ^{10}B below 4.774 MeV are all accompanied by gamma-ray cascades through the intermediate levels. The corresponding gamma-ray yield is greater than the neutron yield for these transitions. The gamma-ray emissions corresponding to a triplet of levels in ^{10}B around 5.2 MeV are not seen in the spectrum. However, it must be noted that all levels above 4.774 MeV have an α-decay mode. This accounts for the low intensity of the gamma-rays from the transitions involving level 8, in spite of the strength of this channel in the neutron spectra. The relative gamma-ray to neutron yield ratio measured for E_d = 4.0 MeV is 1.6.

4.1.3 Conclusions

The ^{9}Be(d,n)^{10}B reaction is a very convenient choice for applications where large neutron fluxes are required and the neutron energy is of secondary importance. The large positive Q-value results in several neutron groups that are always produced in transitions to the lowest levels of the residual ^{10}B nucleus. The reaction yield is dramatically enhanced when the incident deuterons are accelerated beyond 1 MeV, resulting in excitation of one or more of the triplet levels at 5.11, 5.163 and 5.18 MeV in the ^{10}B nucleus. The yield of these low energy neutrons is significantly higher than the yield of the higher energy neutrons resulting from transitions to lower levels in the ^{10}B nucleus. The maximum energy of these low energy neutrons can be controlled by the energy of the incident deuteron. When a thick target is used, a uniform spectrum of neutrons is produced with a low component of neutrons at the higher energies.

The significant gamma-ray production resulting from the ^{9}Be(d,n)^{10}B reaction is of particular importance for applications in radiography. Neutron production is accompanied by cascades of gamma-rays with energies above 1 MeV that result in a gamma-ray per neutron ratio of nearly 2. Since most of the image detectors used for radiography are sensitive to gamma-rays a significant contrast degradation due to the gamma-ray component of the beam can be expected in such systems.

4.2 ^{7}Li(d,n)^{8}Be

The thick target ^{7}Li(d,n)^{8}Be reaction at low incident deuteron energies is quite prolific, nearly matching the yield of the more often used ^{9}Be(d,n)^{10}B reaction, at incident deuteron energies below 10 MeV. Due to the high Q-value of +15.03 MeV the neutron spectrum extends to high energies even if the incident particle is at a relatively low energy. The neutron producing channels in bombardment of ^{7}Li with relatively low energy deuterons are presented in Table 5.

Reaction	Q-value [MeV]
^{7}Li(d,n)^{8}Be	+ 15.03
^{7}Li(d,α)^{5}He	+ 14.2
^{5}He – ^{4}He + n	+ 0.89
^{7}Li(d,pn)^{7}Li	- 2.2
^{7}Li(d,2n)^{7}Be	- 3.9

Table 5. Nuclear reactions contributing to neutron production in bombardment of ^{7}Li with low energy deuterons.

The main disadvantage of Li as a target material is its low melting temperature of 179°C, which in practice severely limits the beam power that can be used with such targets. It was however recently reported that for a special design of the target assembly and enhancing the surface area for heat transfer, it was possible to dissipate 50 kW of beam current in the lithium target and sustain its long-term integrity [23].

Neutron spectra and yields have previously been measured in the deuteron energy range well above 10 MeV for this reaction [58-60]. The details of neutron and gamma-ray production at low incident deuteron energies are not available in the literature.

4.2.1 Neutron Production

A TOF spectrum for a deuteron beam of energy 4.0 MeV, incident on a thin Li target is presented in Figure 11.

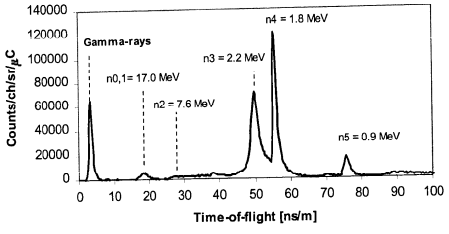


Figure 11. Time-of-flight spectrum obtained in bombardment of a thin Li target with a 4 MeV deuteron beam at 0°. Neutron groups corresponding to different final states of the residual ^{8}Be nucleus are indicated.

As many as 5 neutron groups corresponding to various residual states of ^{8}Be (Figure 12) were resolved in the thin target spectrum: $n_{0,1}$ = 17.0 MeV ($^{8}Be(0,1)$ = 0, 2.94 MeV), n_2 = 7.6 MeV ($^{8}Be(2)$ = 11.4 MeV), n_3 = 2.2 MeV ($^{8}Be(3)$ = 16.627 MeV), n_4 = 1.8 MeV ($^{8}Be(4)$ = 16.911 MeV) and n_5 = 0.9 MeV ($^{8}Be(5)$ = 17.642 MeV).

The neutron continuum of relatively low intensity, due to multi-body reactions detailed in Table 5, is also seen in the spectrum.

The thick target spectra for deuteron beams of energy of 0.9, 1.5 and 4.0 MeV, obtained at laboratory angles of 0°, 40°, 80° and 120° are presented in Figures 13a-13c.

The broad characteristics of the ^{7}Li(d,n)^{8}Be reaction are similar to the characteristics of the ^{9}Be(d,n)^{10}B reaction, except that the strong, low energy neutron group only appears after the channels through levels 3 (16.627 MeV) and 4 (16.911 MeV) in ^{8}Be are open.

Due to the high reaction Q-value, all neutron spectra extend well above 14 MeV with two broad peaks around 3 MeV and 12 MeV. These peaks result from emission of neutron groups corresponding to the second excited state at 11.4 MeV (3 MeV neutron peak) and to the ground state and the first excited state at 2.94 MeV (12 MeV neutron peak) in the residual ^{8}Be nucleus.

There is a dramatic change in the spectral shape for the spectrum obtained with deuteron energy of 4.0 MeV. This is due to the appearance of the neutron groups leaving ^{8}Be in final states at 16.627 MeV and 16.911 MeV. These low energy neutrons dominate the spectrum and significantly increase the overall reaction yield.

The Li(d,n) thick target neutron yields are presented in Table 6.

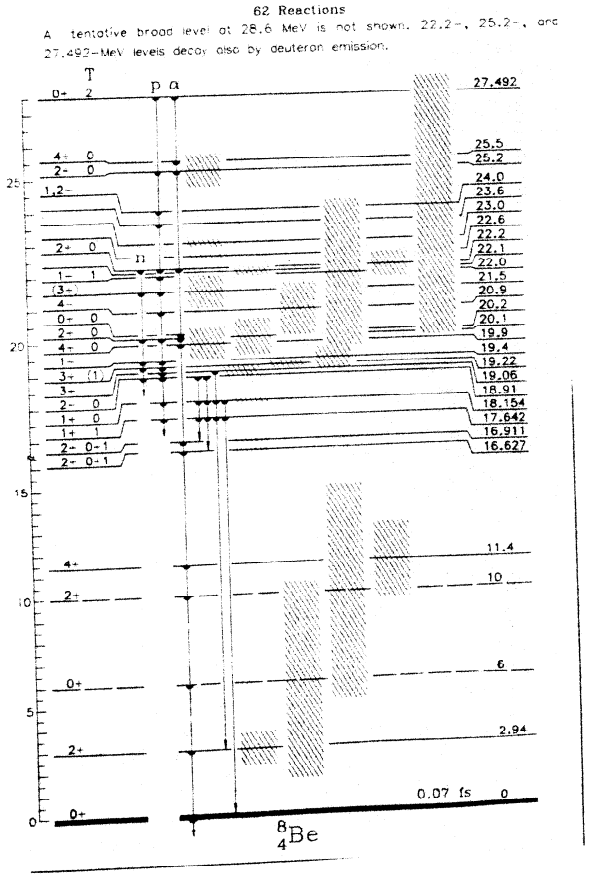


Figure 12. Nuclear level structure of ^{8}Be [80].

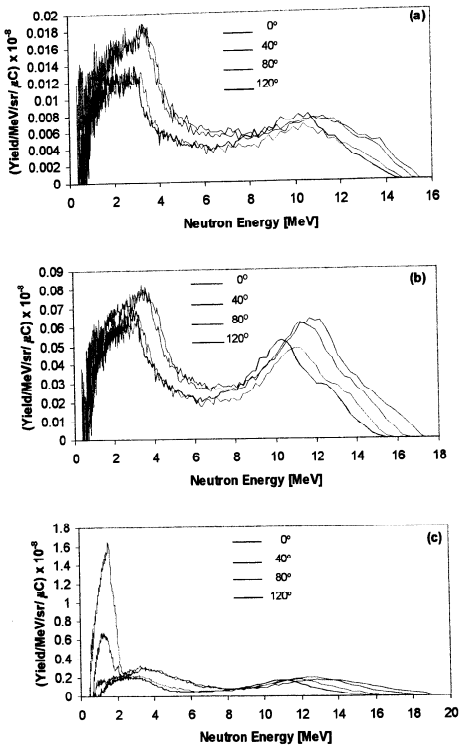


Figure 13. Neutron spectra obtained in bombardment of thick Li target with 0.9 (a), 1.5 (b) and 4.0 (c) MeV deuterons, for various laboratory angles.

Laboratory Angle [Deg]	(Neutron Yield / MeV/ sr / μC) x 10^{-8}		
	E_d = 0.9 MeV	E_d = 1.5 MeV	E_d = 4.0 MeV
0	4.1	0.68	0.12
40	3.0	0.64	0.11
80	1.9	0.48	0.08
120	1.5	0.48	0.08

Table 6. Neutron yield for the thick target Li(d,n) reaction for deuteron energies of 0.9, 1.5 and 4.0 MeV, at various laboratory angles.

4.2.2 Gamma-ray Production

The TOF-gated gamma-ray spectrum, obtained in the bombardment of a thick Li target with 4.0 MeV deuterons is presented in Figure 14. The major gamma-ray lines are identified.

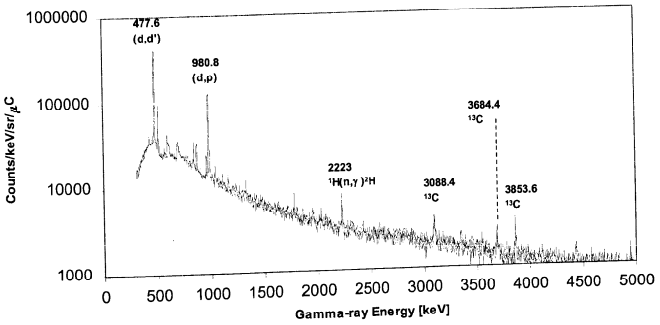


Figure 14. TOF-gated gamma-ray spectrum at 40° obtained in the bombardment of a thick Li target with 4.0 MeV deuterons. The major gamma-ray lines are identified in keV.

The spectrum is dominated by the 477.6 keV and 980.8 keV lines that result from transition to the ground state from the first excited levels in ^{7}Li and ^{8}Li, respectively. These are due to the following nuclear reactions: ^{7}Li(d,d')^{7}Li* and ^{7}Li(d,p)^{8}Li (Q = - 0.192 MeV). Also identifiable are gamma-ray lines originating from shielding materials: 2223 keV and hydrocarbons present in the vacuum system: 3088.4, 3684.4 and 3853.6 keV, resulting from de-excitation of the ^{13}C. There are no gamma lines generated in the de-excitation of the residual ^{8}Be nucleus because all the levels below 17 MeV decay by α emission.

The total gamma-ray yield at deuteron energy of 4.0 MeV was measured as ~ 2 x 10^{8} gamma-ray photons / keV / sr / μC. Comparing this result with the neutron yield (Table 6), there is one gamma-ray photon produced for every neutron, at deuteron energy of 4.0 MeV. Most of these are at the relatively low energy of 477.6 keV.

4.2.3 Conclusions

The ^{7}Li(d,n)^{8}Be reaction exhibits very similar characteristics to the ^{9}Be(d,n)^{10}B reaction. The very large positive Q value results in neutron spectra extending well above 14 MeV, with the two distinct neutron peaks corresponding to the first three excitation states of the residual ^{8}Be nucleus. The neutron yield in the lower energy range is significantly enhanced when the excited states at 16.627 MeV and 16.911 MeV in the residual ^{8}Be nucleus are populated. The neutron yield is only marginally lower than that for the ^{9}Be(d,n)^{10}B reaction.

There is approximately one gamma-ray photon produced per neutron with the major gamma-ray component below 1 MeV, which makes the ^{7}Li(d,n)^{8}Be reaction a potentially better choice for applications in high energy neutron radiography than the ^{9}Be(d,n)^{10}B reaction. However, the poor thermal properties of Li metal severely limit its applications with high current accelerators.

5. CHARACTERIZATION OF THE ^{9}Be(p,n)^{9}B AND ^{7}Li(p,n)^{7}Be REACTIONS

5.1 ^{9}Be(p,n)^{9}B

Interest in the thick target ^{9}Be(p,n)^{9}B reaction at low incident proton energies has recently increased due to its potential for the application in cancer treatment by BNCT. The reaction can also be used as a quasi mono-energetic neutron source for proton energies below 4 MeV. The good thermal properties of the metallic Be target allow it's use at high particle beam currents. The negative Q-value of –1.85 MeV results in the neutron spectrum not exceeding 2.5 MeV if the incident proton beam energy is kept below 4 MeV. The neutron producing channels in bombardment of ^{9}Be with relatively low energy protons are presented in Table 7.

Reaction	Q-value [MeV]
^{9}Be(p,npα)^{4}He	- 1.57
^{9}Be(p,np)^{8}Be	- 1.67
^{9}Be(p,n)^{9}B	- 1.85
^{9}Be(p,pα)^{5}He	- 2.67
^{5}He – ^{4}He + n	+ 0.89
^{9}Be(p,nα)^{5}Li	- 3.54
^{9}Be(p,^{5}He)^{5}Li	- 4.40
^{5}He – ^{4}He + n	+ 0.89

Table 7. Nuclear reactions contributing to neutron production in the bombardment of ^{9}Be with low energy protons.

Neutrons resulting from multi-body reactions may have energies higher than the ground state neutrons of the ^{9}Be(p,n)^{9}B reaction because thresholds for break-up processes occur at a lower energy, as shown in Table 7.

The Be(p,n) reaction has been investigated previously, mostly for an incident proton energy range above 10 MeV [56-60, 81, 82], but the data is very fragmented. Apart from work in the early 1950's and 1960's [83]

and a recent publication by Howard *et al.* [68], there is little data describing the reaction at low incident proton energies, especially for thick target neutron and gamma-ray spectra and yields.

The aim of this work was to establish the range of proton energies in which the reaction can be used as a quasi-mono-energetic neutron source, as well as to investigate neutron and gamma-ray spectra and yields for selected proton energies in thick target reactions.

5.1.1 Neutron Production

The broad features of neutron production in the relevant incident proton energy range may be discussed on the basis of the TOF spectra obtained with thin Be targets. The experimental work for $E_p > 4.0$ MeV was carried out on the 6 MV tandem Van de Graaff accelerator located at the Schonland Research Centre for Nuclear Sciences (SRCNS). Three ns proton pulses were incident on 7.5 μm and 15 μm thick Be targets on a Ta backing at a repetition rate of 2 MHz. The TOF detector, described previously, was biased at 550 keV of proton recoil energy and was used in the electronics set-up presented in Figure 1.

The TOF spectra obtained by bombardment of the 7.5 μm thick Be target with proton beams of energies of 3.0 and 3.8 MeV are presented in Figure 15 (note the logarithmic scale).

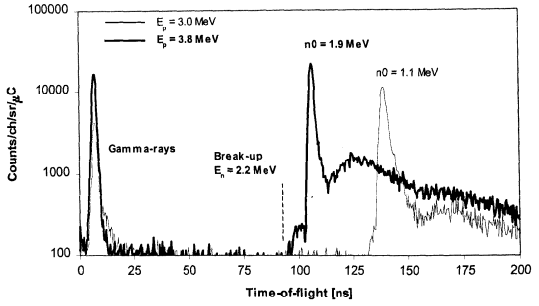


Figure 15. Time-of-flight spectra obtained in the bombardment of a 7.5 μm thick Be target with 3.0 MeV and 3.8 MeV protons. Flight path = 2 m, timing resolution ~ 2 ns. Ground state neutrons are labelled *n0* and maximum energy of break-up neutrons is also marked (E_n = 2.2 MeV for E_p = 3.8 MeV).

The mono-energetic peaks arising from ground state neutrons occur at E_n = 1.1 MeV and 1.9 MeV for E_p = 3.0 and 3.8 MeV, respectively. The broadening of the peaks is a result of the slowing-down of the incident proton within the target material. For a target thickness of 7.5 μm, TRIM [84] calculations indicated neutron energy spreads of 115 keV and 138 keV for for E_p = 3.0 and 3.8 MeV respectively. These are in very good agreement with the measured values.

Also clearly seen is a neutron continuum underlying the mono-energetic peaks that results from the multi-body break-up processes. The maximum energy of break-up neutrons for E_p = 3.8 MeV is 2.2 MeV, and is higher than that of the ground state neutrons due to lower thresholds for break-up reactions. The relative contribution of the break-up neutrons to the overall yield is however not significant in this energy range.

The TOF spectra obtained in the bombardment of the 15 μm thick Be target with protons in the energy range of 4.55 – 9.95 MeV are presented in Figures 16a – 16c.

At E_p = 4.55 MeV the spectrum is still dominated by the mono-energetic peak, corresponding to ground state neutrons that is superimposed on the break-up neutron continuum. There is no evidence of a neutron group corresponding to the controversial 1.68 MeV level in ^{9}B (Figure 17).

The second neutron group corresponding to the 2.361 MeV excited state in ^{9}B becomes evident in the spectrum for E_p = 5.65 MeV. The yield of the second neutron group increases steadily with increasing proton energy and eventually equals the yield of the ground state neutrons at E_p = 9.95 MeV. The yield of the break-up neutrons becomes important for $E_p > 4$ MeV and becomes a dominant part of the spectra for E_p = 6.5 MeV. Only the ground state and 2.361 MeV levels in ^{9}B are populated for $E_p < 10$ MeV.

The background neutron spectrum resulting from interactions of protons with the tantalum backing of the target, at E_p = 9.95 MeV, is presented in Figure 18.

The broad continuum of neutrons results from the ^{181}Ta(p,n)^{181}W reaction (Q = - 0.97 MeV) and proton slowing-down and straggling processes. The cross section for this reaction is small at lower proton energies and rises rapidly to reach a maximum of 100 mb at E_p = 9.5 MeV [85]. The contribution of Ta(p,n) neutrons is insignificant for $E_p < 9$ MeV.

The high relative intensities of gamma-ray peaks in TOF spectra obtained with 7.5 μm target (Figure 15), in comparison with those obtained using a 15 μm target (Figures 16a-16c), are due to interactions of protons with the permanent copper support of the thinner target.

The thick target neutron spectra were obtained at proton energies of 2.57, 3.0 and 4.0 MeV and are presented in Figure 19a-19f.

The lower neutron energy cut-off at 250 keV is due to the detector bias. The maximum energies of the ground state neutron groups are 0.65, 1.10 and 2.12 MeV for E_p = 2.57, 3.0 and 4.0 MeV, respectively. The presence of neutrons at energies higher than the maximum ground state energy is clearly evident in the

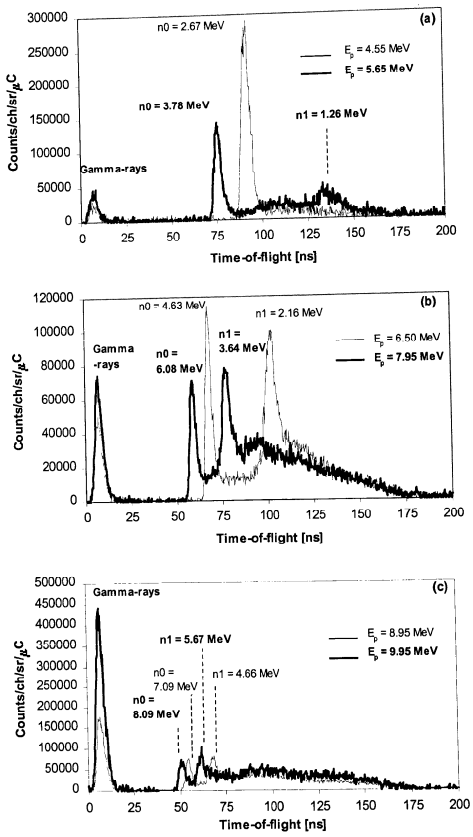


Figure 16. Time-of-flight spectra obtained in the bombardment of a 15 μm thick Be target with protons in the energy range of 4.55 – 9.95 MeV (a – F_p = 4.55 and 5.65 MeV, b – E_p = 6.50 and 7.95 MeV and c – E_p = 8.95 and 9.95 MeV,). Flight path = 2 m, timing resolution ~ 3 ns. Ground state and the first excited state neutron groups are indicated by *n0* and *n1*, respectively.

23 Reactions

Levels above 17 MeV decay also by ^{3}He emission. The 17.19– and 17.64–MeV levels decay also by deuteron emission.

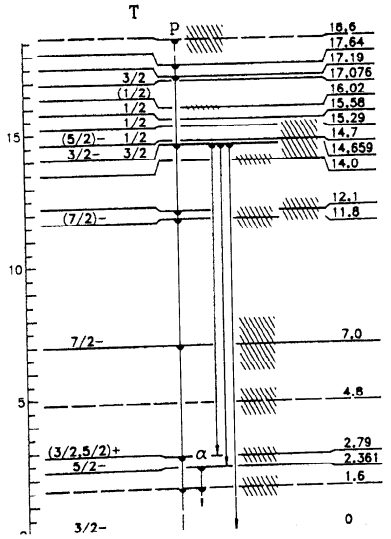


Figure 17. Nuclear level structure of ^{9}B [80].

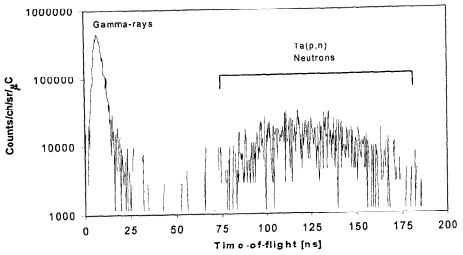


Figure 18. TOF spectrum obtained in the bombardment of thick Ta target with 9.95 MeV protons. Flight path = 2 m, timing resolution ~ 3 ns.

spectrum for E_p = 4.0 MeV (Figure 19e). The neutron group corresponding to the first excited state in ^{9}B is also seen in the same spectrum at 0.31 MeV. This level is not excited for E_p = 2.57 and 3.0 MeV.

The neutron peak at around 0.6 MeV, seen in all the spectra presented in Figure 19, results from the decay of the compound ^{9}B* nucleus, produced by the Be(p,p') reaction. For all the measured spectra the maximum energy of neutrons resulting from the ^{9}Be(p,n)^{9}B reaction decreases with increasing laboratory angle, as predicted by kinematic calculations, whilst the total neutron yield is significantly enhanced by the presence of break-up neutrons.

The Be(p,n) thick target yields, for $E_n \geq 0.25$ MeV, are presented in Figure 20.

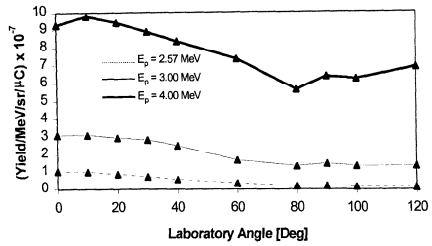


Figure 20. Neutron yield ($E_n \geq 0.25$ MeV) for the thick target Be(p,n) reaction for E_p = 2.57 MeV, 3.0 MeV and 4.0 MeV.

For all the investigated proton energies the maximum yield is observed near 0°. It decreases with increasing laboratory angle and reaches a minimum around 80°, at angles in the range from 80° to 120° it increases again.

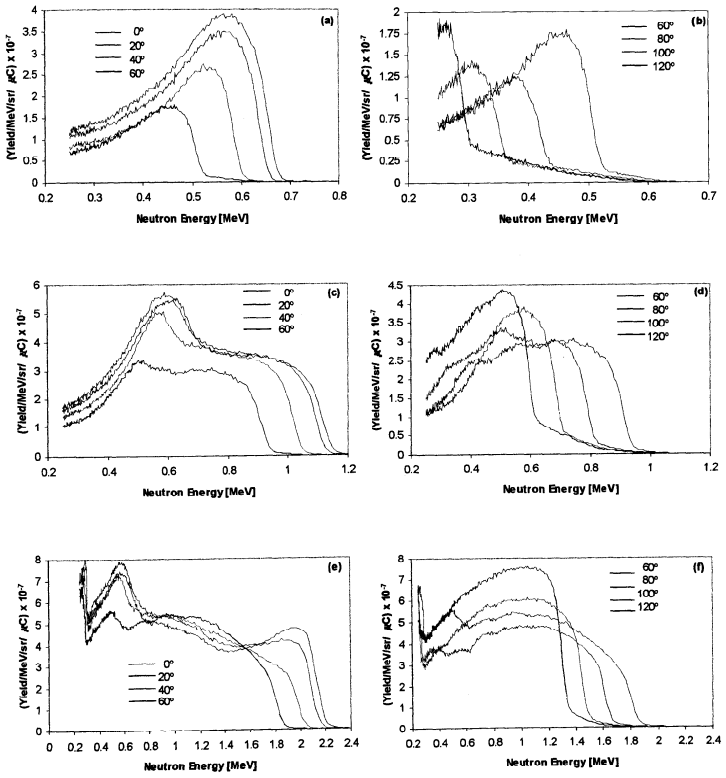


Figure 19. Neutron spectra in the laboratory angle range of 0°-120° obtained in the bombardment of a thick Be target with 2.57 (a,b), 3.0 (c,d) and 4.0 MeV (e,f) protons.

5.1.2 Gamma-ray Production

The TOF-gated and ungated gamma-ray spectra obtained in bombardment of thick Be with 4.0 MeV protons are presented in Figures 21a and 21b. The major gamma-ray lines are identified.

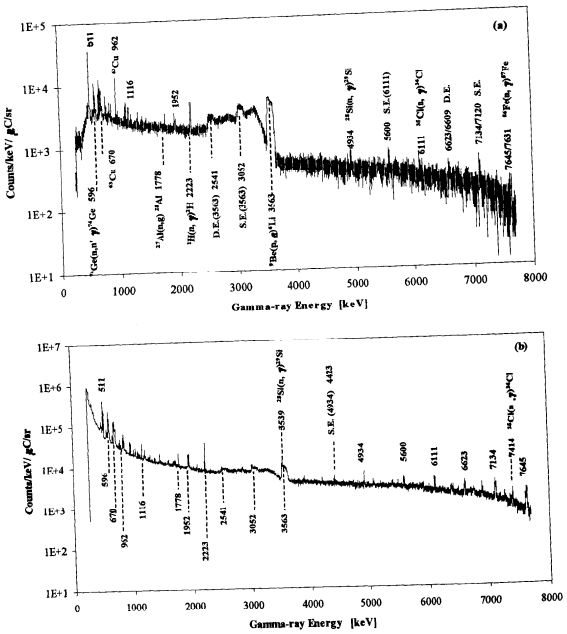


Figure 21. TOF-gated (a) and ungated (b) gamma-ray spectra at 40°, obtained in the bombardment of a thick Be target with 4.0 MeV protons. The major gamma-ray lines are identified in keV.

The TOF-gated spectrum, which represents gamma-ray emission from the target area during the proton beam pulse, is dominated by the Compton scatter background from high energy gamma-rays. Strong 511 keV annihilation peak and the heavily Doppler-broadened peak centered around 3570 keV and its first and second escape peaks.

The Doppler broadened line results from the $^{9}Be(p,\alpha)^{6}Li$ reaction (Q = - 2.126 MeV) leaving ^{6}Li in the excited state at 3563 keV, which subsequently decays by gamma-ray emission. No other gamma-ray lines that result directly from proton interactions in Be were identified.

Other major gamma-ray lines include proton-induced prompt emission from the copper target holder (669, 691.3 and 962.2 keV), neutron-induced lines in the Ge crystal of the detector (596.4, 595.8 and 868.4 keV) and construction materials in the vicinity of the target and detector: 1778 keV from $^{27}Al(n,\gamma)^{28}Al$ and $^{28}Si(n,n'\gamma)^{28}Al$, 847.1 keV from $^{56}Fe(n,n'\gamma)^{56}Fe$ and, notably, the 2223 keV line from $^{1}H(n,\gamma)^{2}H$.

Also seen are high energy (E_γ > 4 MeV) gamma-ray peaks resulting from neutron interactions with surrounding materials. These peaks result from time-uncorrelated interactions and are significantly suppressed by the TOF-gate but are clearly visible in the ungated spectrum. The following lines are identified: 3539 and 4934 keV from ^{28}Si, 6110.9 and 7413.8 keV from ^{35}Cl and 7278.8 and 7645.5 keV from ^{56}Fe, which are all accompanied by the first and second escape peaks. Similar gamma-ray lines are observed in gamma-ray spectra obtained in the bombardment of thick Be with 2.57 and 3.0 MeV protons.

The gamma-ray yields (for 260 keV < E_γ < 8191 keV) were measured for all incident proton energies after correction of the spectra for the detection efficiency. The results, presented in Table 8, indicate that there is less than one gamma-ray photon per neutron produced in the thick target Be(p,n) reaction, at the energy range investigated.

E_p [MeV]	Gamma-ray yield [γ/keV/μC/sr] x 10^{-7}	
	TOF-gated	Ungated
2.57	0.82	8.51
3.00	2.15	25.5
4.00	6.56	86.6

Table 8. Gamma-ray yield (260 keV < E_γ < 8192 keV) at 40° for a thick target Be(p,n) reaction for E_p = 2.57, 3.0 and 4.0 MeV.

This ratio dramatically changes if all gamma-rays, including secondary effects, are counted, and depends on the specific operating conditions of the experiment. In the experimental conditions described in this thesis and in the proton energy range under consideration this ratio was approximately 10 gamma-ray photons per neutron produced.

5.1.3 Conclusions

The $^{9}Be(p,n)^{9}B$ reaction can be used as a quasi mono-energetic fast neutron source in the proton energy range below 4.5 MeV. In this energy range the neutron yield results from the strong emission of the single neutron group corresponding to the ground level of residual ^{9}B nucleus and a relatively low intensity neutron continuum that results from multi-body break-up reactions. The break-up neutrons have energies higher than the ground state neutrons due to lower reaction thresholds. Hence, the $^{9}Be(p,n)^{9}B$ reaction can replace the more often used $^{7}Li(p,n)^{7}Be$ for $E_p < 4.5$ MeV, in applications where large proton current is required.

The second neutron group emerges at $E_p > 4.5$ MeV and increases in intensity with increasing proton energy. The break-up continuum yield also increases steadily and dominates the spectrum for $E_p > 7$ MeV.

The gamma-ray spectrum is dominated by the Doppler-broadened 3563 keV line that results from the excitation of the ^{6}Li nucleus in the $^{9}Be(p,\alpha)^{6}Li$ reaction. There is less than one gamma-ray photon produced per neutron in the thick target reactions.

5.2 $^{7}Li(p,n)^{7}Be$

The $^{7}Li(p,n)^{7}Be$ reaction (Q = -1.644 MeV) is one of the most often used reactions for a source of quasi mono-energetic neutrons of energies up to 4 – 5 MeV. The reaction produces a single neutron group from an incident proton energy threshold from 1.881 MeV up to 2.4 MeV. Above 2.4 MeV bombarding energy, the first excited state of ^{7}Be at 0.43 MeV is excited and results in a second neutron group. However, for $E_p < 5$ MeV, the yield of the second neutron group is always less than 10% of the yield of the ground state neutron, and therefore the mono-energetic character of the reaction is only slightly compromised. The usefulness of the $^{7}Li(p,n)^{7}Be$ reaction as a source of mono-energetic neutrons above 5 MeV bombarding energy is limited due to multi-body break-up reaction of $^{7}Li(p,n^{3}He)^{4}He$ (Q = - 3.69 MeV), which produces a continuum of slow neutrons. In addition, the yield of the second neutron group also increases rapidly as bombarding energies increase even further and a third neutron group appears at a proton energy of 7.11 MeV due to excitation of the 4.57 MeV level in ^{7}Be.

A contribution from $^{6}Li(p,n)^{6}Be$ reaction (Q = - 5.92 MeV) may be seen at higher bombarding proton energies, due to the presence of ^{6}Li in the natural metal (7.5% isotopic abundance).

The experimental data prior to 1973 was evaluated by Liskien and Paulsen [77], for proton energies up to 7 MeV. More recent data were compared by Drosg [55] who observed some minor discrepancies with previous work. Neutron intensities and energy distributions for protons below 5.5 MeV incident on a thick Li target were calculated by Clayton and Spackman [86].

Natural Li metal oxidises easily and care has to be taken when mounting such targets on to the beam-line. Oxidation results in a significantly lower neutron yield and contamination neutrons. Lithium fluoride (LiF) is often used as a target material due to its better chemical stability compared to pure Li metal. This, however, results in a factor of three decrease in neutron yield compared with pure metal target [87]. In addition, the contribution of neutrons from $^{19}F(p,n)^{19}Ne$ (Q = - 4.021 MeV) reaction is not negligible [87].

The pure natural Li targets that were used in this work were prepared by vacuum deposition of a suitable thickness of the metal onto the Ta backing. It was and subsequently covered with a 3 μm thick Havar foil to prevent oxidation. This resulted in slowing-down of the proton beam within the foil material. The interactions between protons and Havar contributed to the gamma-ray emission.

5.2.1 Neutron Production

The TOF spectra obtained in bombardment of thin natural Li targets with 2.36 and 3.70 MeV protons are presented in Figure 22a and 22b.

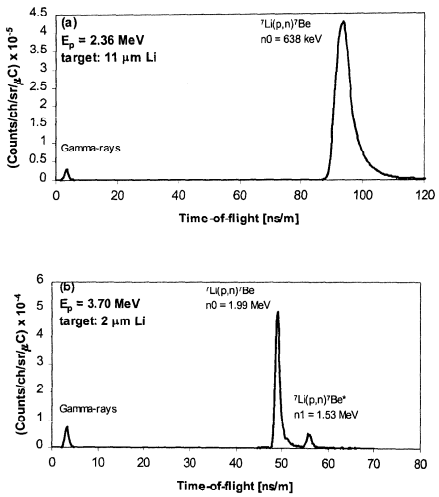


Figure 22. TOF spectra obtained at 0° in the bombardment of a thin natural lithium targets with 2.36 MeV (a) and 3.70 MeV (b) protons.

The single neutron group, at E_n = 638 keV, corresponding to the ground state of ^{7}Be, is the only group seen in the spectrum obtained with E_p = 2.36 MeV, while the two separate neutron groups at E_n = 1.99 and 1.53 MeV, are seen in the spectrum obtained with E_p = 3.70 MeV. These two neutron groups correspond to the ground state and the first excited state of the ^{7}Be residual nucleus (Figure 23). Clearly, the yield of the second neutron group is significantly lower than that of the ground state neutrons. The neutron energy spread observed in both spectra is due to the slowing-down processes of the protons, while traversing the target. The measured values of ~ 70 keV (Figure 22a) and ~ 95 keV (Figure 22b) agree very well with the TRIM [84] calculations.

The neutron spectra obtained at a range of laboratory angles in the bombardment of the thick natural Li target with a proton beam of energy of 2.32 MeV are presented in Figure 24a and 24b.

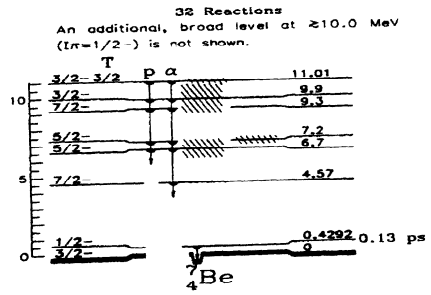


Figure 23. Nuclear level structure of ^{7}Li [80].

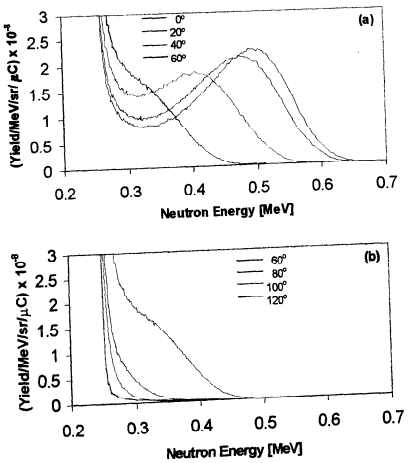


Figure 24. Neutron energy spectra obtained in the bombardment of a thick natural Li target with protons of energy of 2.32 MeV in a range of laboratory angles of 0° – 120°.

The spectra show a single neutron group folded with the proton slowing-down in the target material. The rapid increase of the slow neutron yield at $E_n \sim 300$ keV is a result of a sharp resonance in the reaction cross-section at $E_p \sim 2.25$ MeV (Figure 25).

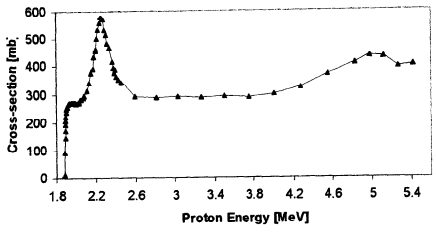


Figure 25. The cross-section for the $^{7}Li(p,n)^{7}Be$ reaction [88].

The total neutron yield, for $E_n > 0.25$ MeV, for thick target Li(p,n) reaction at $E_p = 2.32$ MeV is presented in Figure 26.

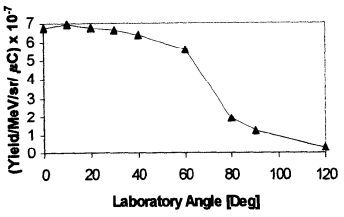


Figure 26. The total neutron yield (for E_n > 0.25 MeV) in the bombardment of a thick Li target with 2.32 MeV proton beam.

The strong forward-peaking of the neutron emission is indicated with the total yield falling by more than a factor of three at laboratory angles greater than 80° in comparison with the 0° yield.

Neutron energy spectra obtained in the bombardment of thick natural Li target with 4.28 MeV protons in the laboratory angle range of 0° – 90° are presented in Figure 27.

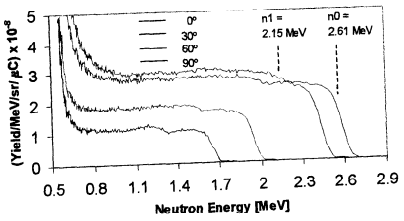


Figure 27. Neutron energy spectra obtained in the bombardment of a thick natural Li target with 4.28 MeV protons in the laboratory angle range of 0° – 90°. The onset energy of the ground state (n0) and the first excited state (n1) neutrons at 0° are indicated in MeV.

These spectra were obtained with the detector bias corresponding to 0.55 MeV of recoil proton energy. The empirical equation proposed by Drosg [89] was used to correct the TOF spectra for detection efficiency:

$$\varepsilon(E,B) = \frac{E-B}{E}\left[1-e^{-t\,n_H\,\sigma_H(E)}\right]\times\left\{1+\frac{B}{E-B/2}\left[1-e^{-1/2\cdot t\cdot n_H\cdot\sigma_H\cdot(E-B/2)}\right]\right\}, \qquad (4)$$

where: $\varepsilon(E,B)$ is the absolute efficiency of the detector, E is the neutron energy, B is the detector bias, t is the detector thickness, n_H is the number of hydrogen atoms per unit volume and σ_H is the total cross section for hydrogen.

The spectra show two distinct neutron groups folded with the proton slowing-down in the target material. The threshold energy for the group associated with the ground state (n0) and the first excited state (n1), for neutrons at 0°, are indicated in MeV. The rapid increase of the slow neutron yield at $E_n \sim 800$ keV is a result of a sharp resonance in the reaction cross-section at $E_p \sim 2.25$ MeV (Figure 25).

The total neutron yield (for $E_n > 0.55$ MeV) is presented in Table 9.

Laboratory Angle [Deg]	Neutron Yield [n MeV^{-1} sr^{-1} μC^{-1}] x 10^{-8}
0	7.5
30	6.4
60	2.9
90	1.5

Table 9. Total neutron yield (for E_n > 0.55 MeV) for a thick natural Li target Li(p,n) reaction.

A very strong forward-peaking of the neutron production is evident.

5.2.2 Gamma-ray Production

The TOF-gated gamma-ray spectrum obtained in the bombardment of a thick natural Li target with 2.32 MeV proton beam at 40° is presented in Figure 28.

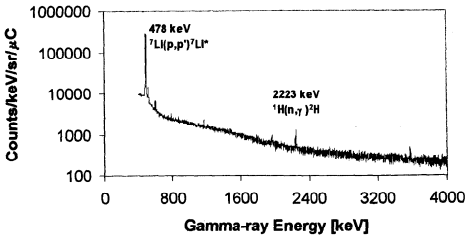


Figure 28. TOF-gated gamma-ray spectrum obtained in the bombardment of a thick natural lithium target with a 2.32 MeV proton beam.

The gamma-ray spectrum is dominated by the 478 keV line resulting from the ^{7}Li(p,p')^{7}Li* reaction. The 2223 keV line from the ^{1}H(n,γ)^{2}H reaction in the shielding material is also clearly seen.

The total gamma-ray yield (for 400 keV < E_γ < 8000 keV) measured at 40° was 2.7 x 10^7 γ sr^{-1} μC and indicated a 3:1 neutron-to-gamma-ray photon ratio at E_p = 2.32 MeV.

5.2.3 Conclusions

The ^{7}Li(p,n)^{7}Be reaction, with a thin lithium target, is a useful source of quasi mono-energetic neutrons in the incident proton energy range below 5 MeV. In spite of the two neutron groups being produced for E_p > 2.4 MeV, the yield of the second neutron group is always less than 10% of the yield of the ground state neutrons, for E_p < 5 MeV, resulting in near-mono-energetic neutron emission.

The low gamma-ray yield in the ^{7}Li(p,n)^{7}Be reaction allows for the production of the high quality neutron beams for nuclear experiments, and for fast neutron radiography in particular. The reaction itself produces almost negligible gamma-ray yield because of the relatively high threshold (2.4 MeV) for the population of the first excited state in the ^{7}Be residual nucleus. The decay of the ^{7}Li* nucleus, resulting from (p,p') reaction produces the 478 keV gamma-rays, which can be easily filtered out. This results in the high quality beams having maximum yield of neutrons of a required energy with minimum contamination by gamma-rays and neutrons of other energies.

The low melting point of Li metal (179°C) is a serious limitation for applications that require high particle beam currents. The use of Li compounds, such as LiF, result in better thermal properties and chemical stability of the target at the expense of netron yield and increased beam contamination.

6. CHARACTERIZATION OF THE $^2H(d,n)^3He$ REACTION WITH GASEOUS TARGETS

The reaction $^2H(d,n)^3He$, known as the D-D reaction, is one of the 'big four' mono-energetic neutron producing reactions and is widely used for the production of neutrons in the 2 – 8 MeV energy range. Practical advantages of the D-D reaction such as the emission of a single, kinematically forward-collimated, neutron group, a large positive Q-value (Q = + 3.27 MeV) and large cross-section for neutron production, make it an ideal choice in applications where large fluxes of mono-energetic neutrons, in the range of several MeV, are required. The usefulness of the D-D reaction as a source of mono-energetic neutrons at energies in excess of 8 MeV decreases because of the appearance of low energy break-up neutrons at a break-up threshold of $E_d = 4.45$ MeV.

There are numerous articles and review papers discussing various aspects of the D-D reaction and its applications. A very comprehensive summary of the D-D reaction characteristics can be found in [53]. The laboratory differential and total cross-sections were calculated by Liskien and Paulsen [78] on the basis of available thin target data. This data was later evaluated by Drosg and Schwerer [55].

The development of accelerator-based intense D-D neutron sources is largely limited by the target system. This is particularly true with modern RFQ linacs and other small accelerators where it is possible to accelerate up to several mA of beam, to energies in the low MeV range, at a relatively low cost. In the design of a suitable target, there is a particular advantage when using the pure elemental form of the material, rather than a mixture or compound, in the nuclear reaction employed. The available particle beam can then be fully utilised. This provides a challenge in the design of targets for those elements that occur in a gaseous state at the operating temperature and pressure of the target.

The D-D and D-T reactions fall into this category. Traditionally these hydrogen-isotope targets have been used in the form of hydrided metals such as titanium or zirconium [48]. A serious problem in this approach is the decrease in neutron yield with prolonged bombardment. In addition, the beam is slowed-down extensively in the metal and only a relatively small fraction is used effectively for the production of fast neutrons. Another approach has been to use a gas cell with a thin window, typically a thin metallic foil. A number of ingenious developments of this approach have been reported [90-94] but in high intensity applications it is fundamentally limited by the ability of the window to withstand high beam currents and high target pressures. In addition, reactions resulting from interactions of the beam with the window material produce gamma-rays and complicate the emitted neutron spectrum. Heavy water targets meet the beam power dissipation requirements but, as well as hydrided metal targets, suffer from lower neutron output, large neutron beam energy spread and, most important, a large degree of neutron beam contamination, due to the presence of oxygen [95, 96].

In the case of deuterium, a windowless gas target has many potential advantages. There is no loss of beam energy either in a window or in a matrix material, so that the maximum neutron output is achieved per

MeV of the accelerated beam energy. In addition, power dissipation in the target is effectively handled through the heat exchange in the gas. The use of a windowless gas target at relatively high pressures involves the use of differentially pumped cells connected by small-bore apertures. The gas load on the system can be very high and as a result the gas pressures reported in the literature for such targets with plain orifices are limited to about 100 mbar [97-101]. A variation of this approach has used a supersonic jet to create a highly localized high pressure target zone while capturing most of the jet in a suitable exhaust to reduce the pumping load on the differentially pumped system [102-109]. However, a very high feed pressure is required to achieve a suitable density in the target zone. There is also a need for the jet zone to be small, in order to create a high-density region with a reasonable recirculation load on the compressor, and this tends to limit the overall reaction yield.

In the case of an accelerator operating in a pulsed and bunched mode, a different approach can be adopted. In such an accelerator, for example the RFQ linac, a very high peak current can be combined with a low duty cycle. A suitable shutter mechanism can then be effectively used to isolate the target between beam pulses, and this considerably reduces the gas load on a differentially pumped system while maintaining the target at high pressure. Bonin and McIlrath used this approach to separate gases in a laser application [110] but it can also be used with a pulsed particle accelerator.

Two different designs of the gas target systems were developed for application in this project, i. e., a cooled windowed gas target and a differentially pumped gas target [111]. A description of the two types of gas targets and a comprehensive characterization of the neutron and gamma-ray production, for the two cases follows.

6.1 Cooled Windowed Deuterium Gas Target

6.1.1 Target Design

Information regarding the pressure holding capabilities of metal foil windows of various diameters and foil thickness have been reported in the literature [91, 94, 112, 113]. In most instances relatively thick foils (tens of μm), of several cm^2 in area, are used to withstand intense (10 – 100 μA) high energy (MeV) ion beams. The disadvantage of using thick entrance windows is that they slow-down the incoming ion beam significantly and result in high gamma-ray and slow neutron background contribution. Based on reported experience it was decided from the outset of this work that the superior properties of the metal, Havar, would be used in the development of the gas target. A summary of the physical properties of Havar is presented in Table 10.

Elemental composition [%]

Be	C	Co	Cr	Fe	Mn	Mo	Ni	P	S	Si	W
0.048	0.20	41.65	19.61	19.75	1.55	2.19	12.39	0.002	0.002	0.02	2.59

Physical properties

Tensile strength	965 Mpa	**Melting point**	1480°C
Modulus elasticity	207 Gpa	**Thermal expansion coefficient**	12.5×10^{-6} K^{-1}
Density	8.32 g cm^{-3}	**Thermal conductivity**	13.0 W m^{-1} K^{-1}

Table 10. Properties of Havar [114].

Cooled window gas targets with a grid system to lend extra support to the window [115] indicated that high beam currents could be handled, however this arrangement would be inappropriate in our case due to the high gamma-ray yield that would result from the beam interactions with the grid. Due to the fact that the incident deuteron beam energies were fixed by the type of accelerator to be used any beam energy losses, due to the target window, had to be kept to a minimum.

The energy loss experienced by 1, 3 and 5 MeV deuteron beams traversing various thickness of Havar were calculated using simulation routine TRIM [84] and are presented in Figure 29.

Previous experience with 3 μm Havar foil, 5 mm in diameter, mounted on a 10 cm long gas cell pressurized to 1 bar at room temperature, indicated reliable performance. No failure occurred for extended bombardment times (typically in excess of 400 hours) with a 2.5 μA beam of 5 MeV deuterons focused to a 5 mm diameter spot. The performance of this gas cell acted as a reference for attempts to improve the neutron yield characteristics in a more effective system. Critical aspects in the desired system were:

1. a high neutron yield – as a function of gas pressure and cell length for a given beam energy and current,
2. minimum neutron energy dispersion – specifically at 0° (beam) direction, but also laterally,
3. minimum gamma-ray yield – since the detection system would not be entirely insensitive to the influence of gamma-rays, materials other than the deuterium gas must be kept to a minimum; this implies the use of a thin entrance window.

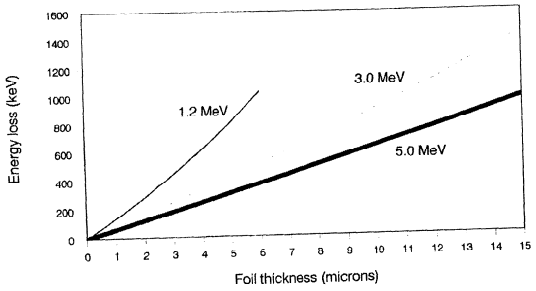


Figure 29. Energy loss of deuteron ions traversing Havar foil as evaluated using TRIM [84].

The deuteron beam generated by the accelerator produced a beam spot of 4 – 5 mm in diameter at a specific focal point. Dispersion of the beam after the focal point was rapid, therefore it was desirable to have as compact a target as possible. This could be attained by increasing the gas pressure, however it was already known that the rupture thresholds were low for the thin Havar to be used.

It has been reported [116] that the pressure at which the window would burst could be raised considerably by decreasing the temperature of the gas – and as a result the temperature of the window itself. When such windows were bombarded with a 8.3 MeV pulsed (800 Hz) deuteron beam current of 120 μA, on a 2 x 2 mm spot, over a 10 mm diameter surface, it was reported that the windows were found to survive for extended periods of time.

The main problem areas encountered with developing an appropriate cooled gas target system were:

1. developing an efficient means of cooling the Havar window,
2. removal of the dumped beam energy (up to 500 W) within the gas cell system, 85% of this is deposited at the end of the gas cell,
3. development of an appropriate closed gas circulation system to accommodate the above conditions.

Molitoris and Nitschke [94] have reported on temperature measurements of 2 μm Havar cooled with liquid nitrogen. The temperature increase being 10°C for 10 W absorption and 100°C for 15 W absorption. As thermal conductance across the foil will be small, one must therefore rely on heat transfer to the gas flowing over the window surface. For the best heat transfer properties the gas flow must be turbulent. On this score, it was also reported that although the cooling properties of the gas improved with increasing gas pressure, this improvement appeared to reach saturation at a pressure differential of around 250 kPa.

A schematic diagram of the gas target system, developed in cooperation with the Atomic Energy Corporation of South Africa (AEC), is presented in Figure 30.

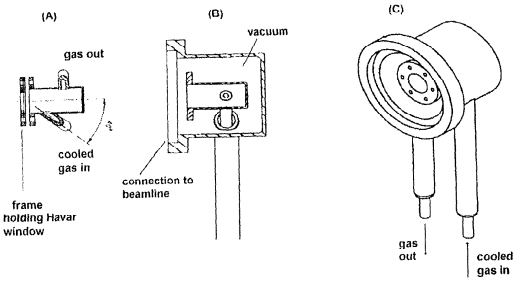


Figure 30. Schematic of the gas cell system.

The window was formed by gluing the foil (Araldite) between two metal plates with apertures with rounded edges. The metal plates were made of 2 mm thick polished stainless steel. The vacuum seal between the frame and the cell was made using an indium o-ring. Several destructive tests were made to confirm the pressure rupture threshold at room temperature.

The results for 2.5 μm Havar foils being $p_{rupture}$ = 200-230 kPa for 11 mm diameter and $p_{rupture}$ = 500-540 kPa for 7 mm diameter, which were consistent with previously reported values [111]. Predictions for a steady state condition, assuming a beam of 3 mm diameter passing through a Havar window of 5 mm, diameter were calculated. Forced convection cooling with a heat-transfer coefficient of 0.2 W cm^{-1} $°C^{-1}$ was assumed as well as a temperature constraint of 20°C imposed on the edge of the window (i. e. using a cooled frame). The resulting temperature profiles for both a uniform beam intensity distribution and a truncated Gaussian distribution for a 4.5 MeV deuteron beam current of 50 μA are shown in Figure 31.

As can be seen, the gaussian profile would result in excessive heating of the window. Inclusion of cooling of the window to liquid nitrogen temperatures was estimated to yield up to a 30% improvement in its beam handling capability.

The target material is deuterium gas, which is also the coolant for the Havar window. For a beam current, $I_{\mu A}$, there will be gas heating due to the 5 MeV deuteron beam from the following sources:

1. heat exchange from the window; for 2.5 μm Havar, will be 0.15 x $I_{\mu A}$ watts,
2. heat deposition in the gas due to the beam; for a 3 cm long gas cell at a mean cell temperature of 120 K and pressure of 100 kPa this will be ~ 0.48 x $I_{\mu A}$ watts,
3. heat transfer from the 1 mm thick Ta beam stop. Due to the fact that minimal material is wanted in the forward direction, the circulating gas was used to conduct the heat away from the beam stop area. The amount of heat to be removed will thus be the residual beam energy ~ 4.37 x $I_{\mu A}$ watts.

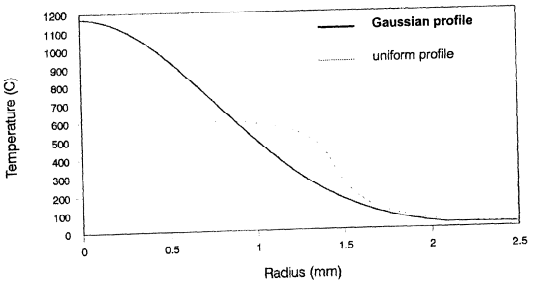


Figure 31. Calculated temperature profiles for Gaussian and uniform beam distribution of 4.5 MeV ions at 50 μA passing through 2.5 μm of Havar. Beam spot size was 3 mm in diameter, foil size was 5 mm in diameter.

Although the primary aim was to cool the gas to the temperature of liquid nitrogen (77 K), heat losses during gas transfer as well as heating of the gas due to the full energy of the beam (E_d x $I_{\mu A}$ watts) would result in a mean gas temperature in a 3 cm long gas cell of ~ 100 K when using a pumping system capable of circulating 2.6 l s^{-1} of deuterium gas.

The energy loss of the deuteron beam passing through 2.5 μm Havar is predominated by electronic interactions with the metallic lattice and will be ~ 140 keV μm^{-1} at 1.2 MeV and ~ 60 keV μm^{-1} at 5 MeV deuteron energy, respectively.

Various tests of the gas target described above were performed using the 3.7 MeV Van de Graaff accelerator at the laboratories of the AEC. In summary, it became evident that reproducible foil behavior

could be obtained and that irradiating a cooled window of 11 mm in diameter with 1.2 MeV deuteron beam current of 19 μA, focused to a diameter of 5 mm (equivalent to 49 μA of 5 MeV deuteron beam), could be sustained for in excess of 6 hours. Increasing the current above these values resulted in rapid foil failure.

6.1.2 Neutron and Gamma-ray Production

The TOF characterization of the gas target developed was performed using a 5 MeV deuteron beam at an average current of 1.5 μA. The standard set-up described in section 2.1 was used.

A static gas cell, 10 cm long, with 3 μm Havar window was used for comparison of neutron and gamma-ray spectra. Reliable performance of this gas target was established for average currents of 1.5 μA, 5 MeV deuteron beams, up to a static pressure of the deuterium gas of 1.5 bar. TOF spectra obtained for different gas pressures are presented in Figure 32.

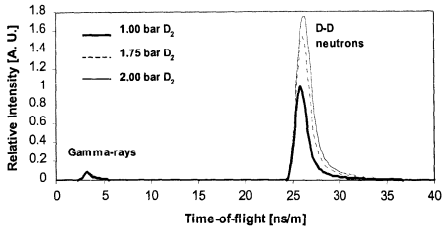


Figure 32. TOF spectra at 0° obtained from the bombardment of the reference gas cell (10 cm long, 3 μm Havar foil, deuterium at room temperature) at different static pressures of deuterium gas, with a 5 MeV deuteron beam. The maximum value in the neutron peak in the spectrum for 1 bar deuterium pressure was normalized to unity.

An increase in neutron yield and neutron energy spread with increasing gas pressure is evident. Whereas the gamma-ray yield remained unchanged as it originates in the target construction materials rather than in the deuterium gas.

The origin of the gamma-rays becomes more evident when the TOF spectra obtained with an evacuated gas cell with Havar window and Havar window removed are compared (Figure 33).

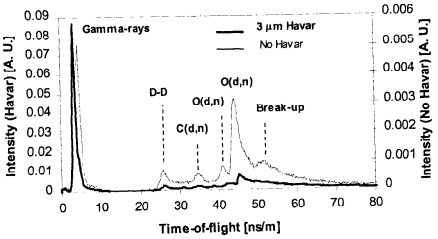


Figure 33. TOF spectra obtained at 0° in the bombardment of an evacuated reference cell with and without Havar entrance foil present. Spectra normalized as in Figure 32.

More than an order of magnitude decrease in gamma-ray yield in the TOF spectrum with no Havar present (also see Figure 34), indicated that the contribution to the gamma-ray yield was largely a result of the interaction of the deuteron beam with the entrance window, with the remainder originating in the end-stop of the cell.

The shift in the gamma-ray peak position on the time-scale, observed in the spectra with and without Havar foil present, corresponds to the time-of-flight of a deuteron beam between the entrance foil and the target end-stop. A relatively small neutron background is evident in the spectra presented in Figure 33. This background consists of three separate components:

1. fast neutrons resulting from the $D(d,n)^3He$ reaction on the deuterium ions implanted into the target end-stop during prolonged irradiation,
2. neutrons from the $^{12}C(d,n)^{13}N$ (Q = - 0.281 MeV) and $^{16}O(d,n)^{17}F$ (Q = - 1.625 MeV) reactions, resulting from contamination of the target gas and surfaces with carbon and oxygen,
3. break-up neutron continuum (small in comparison with the D-D neutron intensity).

The TOF-gated gamma-ray spectra obtained with evacuated reference cell with and without the Havar foil present are presented in Figure 34.

Almost an order of magnitude decrease in gamma-ray background is observed if the Havar foil is removed from the deuteron beam. The energies of gamma-ray lines corresponding to the excitations of various nuclei constituting the foil material (Fe, Cr, Co, Mo and Ni) are marked in keV.

Figure 35 illustrates the TOF spectra obtained for the 10 cm reference cell and newly developed 3 cm cell containing 1 bar of deuterium gas at room temperature and cooled-down to ~ 100 K.

As can be seen, the neutron yield obtained with cooling the gas is about three times higher than when a gas at room temperature was used, and is almost equivalent to the yield of the reference cell. Also clearly seen

is a drop in gamma-ray yield when a 1.5 μm Havar foil rather than a 3 μm foil was used as a beam entrance window (note that the gamma-ray peaks have been multiplied by 10).

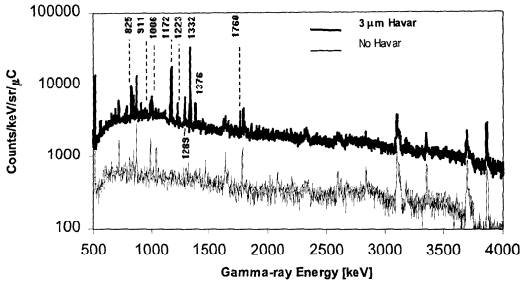


Figure 34. TOF-gated gamma-ray spectra at 0° obtained in the bombardment of evacuated reference gas cell, with and without Havar entrance foil present, with a 5 MeV deuteron beam.

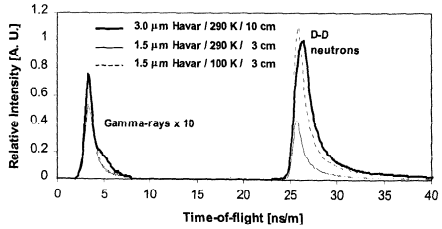


Figure 35. TOF spectra at 0° obtained in the bombardment of the reference cell and newly developed target cell (3 cm long, 1.5 μm Havar foil), filled with deuterium gas at room temperature and cooled-down to 100 K, with a 5 MeV deuteron beam. Spectra normalized as in Figure 32.

The double peak feature observed in the gamma-ray peak for the 10 cm long gas cell iss the result of two subsequent gamma-ray bursts originating in the entrance window (main peak) and the target end-stop. These are separated by the deuteron beam time-of-flight through the length of the cell (~ 4.6 ns). Due to the timing resolution of the system (~ 2 ns) this feature could not be resolved for the shorter, 3 cm gas cell.

The 5 MeV deuteron beam incident on deuterium gas produces 8.1 MeV neutrons with a 2.5 μm Havar foil as the target window (8.15 MeV for 1.5 μm Havar). The neutron energy spreads over ~ 800 keV due to the gas cell length (3 cm), deuterium gas pressure (1 bar) and gas temperature (100 K).

The 0° yield of fast neutrons from the $D(d,n)^3He$ reaction with 5 MeV deuterons was measured as 3.15 x 10^8 n sr^{-1} μC^{-1}, in the 3 cm cell at 1 bar. The maximum 0° output of such a target will therefore reach 1.42 x 10^{10} n sr^{-1} s^{-1} at a beam current of 45 μA.

The background of slower neutrons (E_n < 4.5 MeV) was measured as 2.3 x 10^7 n sr^{-1} μC^{-1}, i.e. about 6 % of the principal neutron group.

The gamma-ray yield varied with the thickness of the Havar foil and was measured as 4.3 x 10^7 γ sr^{-1} μC^{-1} when 2.5 μm foil was used and 3.3 x 10^7 γ sr^{-1} μC^{-1} when 1.5 μm foil was used.

6.1.3 Conclusions

The $^2H(d,n)^3He$ reaction is an ideal choice for production of strictly mono-energetic neutron beams up to the threshold for deuteron break-up at 4.45 MeV, with a maximum neutron energy of 7.8 MeV at a laboratory angle of 0°. In this energy range, neutrons of other energies only originate from the contamination of the target. The break-up neutron yield increases rapidly above the threshold energy.

No gamma-rays are produced in the reaction itself. The gamma-ray yield observed experimentally originates from the construction materials of the target, such as the entrance foil or the target end-stop. It can be minimized by the use of the thin metallic foils for the beam entrance and metals such as tantalum or tungsten as the beam end-stop. The high Coulomb barrier of such metals prevents the nuclear reactions producing background neutrons of energies different from those required for the application.

A particularly serious limitation in the applications of the $^2H(d,n)^3He$ reaction, especially at the high deuteron beam currents, is the necessity of having a target in the gaseous form. The beam entrance foils have to be kept thin in order to minimize the production of the gamma-rays and low energy neutrons, which often causes a catastrophic break-down by the combined effect of the gas pressure and beam heating.

The design of the windowed target finally developed for this project uses a 1.5 μm Havar foil as the beam entrance and tantalum metal as the beam end-stop. The target gas was circulated and cooled to temperatures of 100 K providing an effective mechanism for the dissipation of the particle beam-generated

heat at the entrance foil and the target end-stop. An additional advantage of the cooling of the target gas is the increase of the gas density, which facilitates more compact target design for the required neutron energy spread.

The windowed gas target with a 3 cm long gas cell at 1 bar of deuterium cooled to 100 K with a 1.5 μm Havar foil used as the beam entrance was tested with a 5 MeV deuteron beam. The long term operation of the target could be sustained at the maximum deuteron beam current of 45 μA. This produced 8.15 MeV neutrons with an energy spread of 800 keV and a maximum neutron output of 1.42×10^{10} n sr^{-1} s^{-1} at 0°.

The slow neutron background resulting from deuteron break-up and contamination of the target gas and the gamma-rays resulting from the interaction of the particle beam with the construction materials of the target contributed 6.2 % and 8.9 % to the total reaction yield, respectively.

The design of the gas target described here presents an inexpensive solution to production of substantial neutron outputs for applications in nuclear experiments. The compact structure of the target as well as very low contamination of the primary neutron beam resulting from its operation, makes it particularly useful for applications in fast neutron radiography.

6.2 Differentially Pumped Deuterium Gas Target

6.2.1 Target Design

The fundamental limitations of the beam handling capabilities of a windowed gas target do not allow for its applications where beam currents of the order of hundreds μA and more are required. An alternative approach is to employ a windowless, differentially pumped gas target system. Such systems are significantly more complex and expensive than the windowed targets, but they are far better suited to the high beam current applications.

A differentially pumped gas target has been developed at De Beers Diamond Research Laboratory, Johannesburg, South Africa [111] for use with an accelerator operating in a pulsed and bunched mode, for example the RFQ linac. The concept uses a high speed rotary shutter comprising of a set of spinning disc seals that intermittently close and open orifices in differentially pumped system. The gas target chamber arrangement is schematically illustrated in Figure 36.

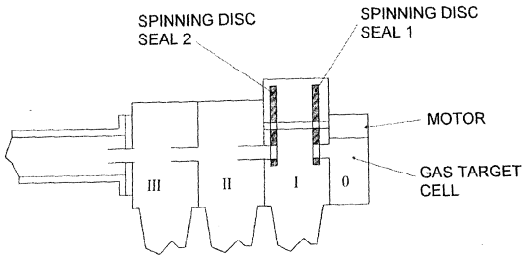


Figure 36. Schematic of the differentially pumped gas target arrangement.

In this design, the target gas is fed into the target cell-0 at the desired pressure (in this case 1 bar). The cell gas is then free to escape through a fixed connecting orifice into the chamber-I. Gas flow is impeded by a disc seal-1 in close proximity to the fixed orifice. Both of these disc seals have three holes drilled in them,

with each hole coming into coincidence with the fixed orifice during rotation of the disc. This allows unobstructed transmission of the ion beam at a frequency in phase with the rotation of the disc.

The effective tube length of the orifice and holes in the disc are made short, to reduce the interface length between the cell and chamber-I. The leakage rate is not adversely affected because the flow is choked at the sonic throat of the orifice. Between coincidences of the holes in the disc and the fixed orifice, the disc limits the gas flow out of the cell through the orifice into chamber-I. The few micron clearance between the disc and the fixed orifice impedes the gas flow.

Similarly, the disc seal-2 acts to limit the gas flow out of chamber-I into the second expansion chamber-II. The orifice and hole lengths are longer in this case, to decrease viscous and molecular conductance. Both disc seals are mounted on a common shaft located in chamber-I to reduce the mechanical complexity and simplify the shaft sealing requirements. The shaft is driven by a DC brushless servo motor located outside the vacuum chamber and sealed using a double radial shaft seal arrangement. The disc seal can rotate at up to 3000 rpm corresponding to a beam repetition rate of 150 Hz.

The orifices connecting chamber-I to –II and chamber-III to the beamline are plain and long, to decrease viscous and molecular conductance. The overall length of the chamber arrangement from the beam line connection to the beginning of the target cell is 360 mm. For this particular configuration the orifice sizes were set to allow a 4 mm diameter focused beam to pass through all the orifices. The beam optics, required the cell orifice to have a 5 mm diameter and the three upstream orifices to have diameters of 5, 6 and 7 mm, respectively. The second orifice was approximately 30 mm long and the third and fourth orifices were each 50 mm long.

Chamber-I was evacuated by a 1000 $m^3 hr^{-1}$ Roots pump, while chambers-II and –III were both evacuated by 500 $l s^{-1}$ turbomolecular-drag pumps. The exhaust from these pumps were fed into chamber-I and then backed by the Roots pump.

The exhaust of the roots pump was fed into a 340 $m^3 hr^{-1}$ oil-sealed rotary vane pump fitted with automatic oil mist elimination and return, followed by cartridge oil filters to reduce oil emission leaving the pump to less than 0.01%.

The exhaust from the oil-sealed rotary vane pump is used to feed the gas cell in a closed circuit recirculation system. This recirculation line is fitted with a gas to liquid heat exchanger to reduce the gas temperature of the exhaust to approximately 20°C prior to transfer into the cell.

The re-circulation line to the target cell is also a point in the circuit where deuterium gas is fed into the system, and where an auxiliary two stage rotary vane pump is inserted to allow for evacuation of the entire system prior to charging the system with the process gas. The system is fitted with valves and instruments to allow for effective control and monitoring of the system performance. The entire gas target and pumping system arrangement is illustrated schematically in Figure 37.

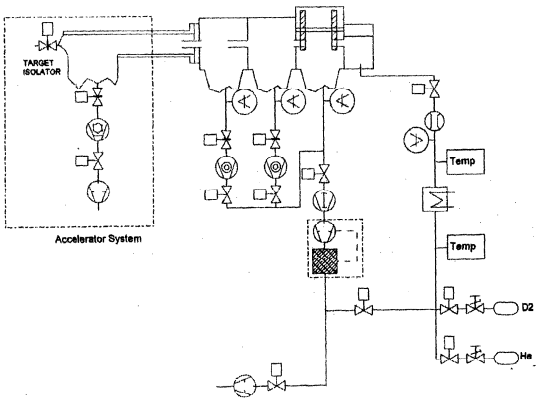


Figure 37. Schematic of the differentially pumped gas target vacuum system.

Synchronization of the disc rotation with the beam was achieved using a transmission infra-red optical pick-up connected to a high speed amplifier. An appropriate delay and triggering system was then used to achieve the transmission of the beam into the target. This signal could also be used for sequencing other peripheral equipment such as detectors.

The disc seal performance characterization was modeled using computational fluid dynamics [111]. During testing, the target successfully operated while coupled to the accelerator and was tested up to a cell pressure of 1.23 bar. This is the maximum pressure to which the exhaust pump could safely pressurize the recirculation line. Typical measured target gas dynamics performance, under different conditions, are shown in Table 11.

Gas Type	P_0 [mbar]	P_I [mbar]	P_0 / P_I	P_{II} [mbar]	P_I / P_{II}	P_{III} [mbar]	P_{II} / P_{III}
Air / N_2	1000	0.71	1408	9.6×10^{-4}	739	3.0×10^{-6}	320
He	1000	2.2	455	7.0×10^{-3}	314	4.9×10^{-5}	142
D_2	1000	1.9	526	4.7×10^{-3}	404	2.0×10^{-5}	235
D_2	1230	2.5	492	5.5×10^{-3}	454	3.1×10^{-5}	177

Table 11. Gas dynamics performance of the differentially pumped gas target system, measured for described geometry with various gases [111].

The system was also tested with a gas bottle feed using He and N_2 gases up to 3 bar absolute since the characteristics of He are very similar to D_2 in the system. With the addition of a suitable compressor, the system could be upgraded to a 3 bar target cell. In order to maintain safe operation of the turbomolecular-drag pumps, the seal gap needs to be carefully set to minimize seal leakage.

The system was found to be very sensitive to any variance in the seal gap size, especially on the first disc seal. A 50 μm gap contributed two thirds of the total leakage in the given configuration and hence, any variation of the gap due to set-up movement would have a significant effect on the upstream pressures. The model was reasonably accurate at predicting the leakage for a pre-determined gap on any disc seal configuration, thus allowing for a parametric study of the gas target system and the final selection of the pumping system equipment without the need to carry out extensive testing [111].

6.2.2 Neutron and Gamma-ray Production

The TOF characterization of the gas target developed was performed using pulsed 2.1 MeV and 5 MeV deuteron beams.

The gas target was operated with the rotating disc seal spinning at 500 rpm (i.e. coincidence rate of holes on the disc seal and fixed orifice of the gas cell = 25 Hz). For this rotation frequency the full open-close period for 5 mm apertures in the gas target opening and the rotating disc seal was only 2.73 ms per cycle. Consequently, less than 2% of the incident deuteron beam was transmitted into the deuterium gas in the gas cell, the remaining majority striking the rotating disc seal.

The standard TOF set-up, as described in section 3.1, was therefore modified to enable gating of the TOF detector with an external gate of variable width and delay, triggered by an infra-red optical pick-up, indicating synchronization of a hole in the rotating disc seal with the gas cell opening. Such a gated TOF spectrum represented the true neutron emission from the target, when the beam repetition rate and the frequency of rotation of the disc seal were matched.

The gated and ungated TOF spectra obtained with the 2.1 MeV deuteron beam incident on the target charged with deuterium gas at 1 bar are presented in Figure 38.

The series of gamma-ray peaks seen in the ungated spectrum correspond to successive gamma-ray bursts that originate during the passage of the incident deuteron beam through various apertures of the gas target system. The numbers indicate the particular aperture hit by the incident beam (compare with Figure 36): *1A* and *1B* representing the entrance and exit zones in chamber-I, *3* and *4* representing rotating disc seal-1 and –2, and *5* representing the Ta end-stop of the target.

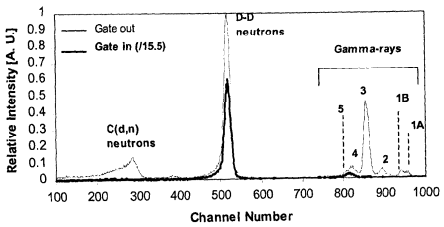


Figure 38. Gated and ungated TOF spectra obtained during the bombardment of the target charged with 1 bar of deuterium gas at room temperature, with 2.1 MeV deuteron beam. Flight distance = 2 m, timing calibration = 0.186 ns ch^{-1}.

As expected, the gamma-ray signal is dominated by the emission from the rotating disc seal, which obstructed the gas cell orifice for some 98% of exposure time.

The following were also clearly seen: the fast neutron peak from then $D(d,n)^3He$ reaction at 3.5 MeV and a background of slow neutrons (E_n < 1.7 MeV) resulting from the $^{12}C(d,n)^{13}N$ reaction (Q = - 0.281 MeV), due to the carbon component of the steel material in the rotating disc and residual hydrocarbons in the beamline from the vacuum pumps.

When the TOF detector was gated with an appropriately delayed gate (100 ms), the TOF spectrum for the beam in coincidence with the rotation of the disc seal was recorded. The gamma-rays in this spectrum originated almost exclusively in the Ta end-stop of the gas cell, with very little beam hitting the apertures of the rotating disc seal. The strong $D(d,n)^3He$ neutron emission dominates the spectrum while the background of the $^{12}C(d,n)^{13}N$ neutrons becomes negligible.

The importance of setting of the external gate width and delay correctly is illustrated in Figure 39, where the gated TOF spectra, obtained in the bombardment of the gas target charged with deuterium gas at 1 bar, using 5 MeV deuteron beam, are presented.

The properly set 100 ms long gate resulted in a clean TOF spectrum with the maximum neutron yield. A wider, 1200 ms long gate with a mismatched delay, enabled a portion of the incident beam hitting the rotating disc seal to be 'seen' by the TOF detector. This resulted in a TOF spectrum with reduced fast neutron output and increased gamma-ray and slow neutron component.

The origin of the slow neutron background (E_n < 4.5 MeV) can be determined by comparison of TOF spectra presented in Figure 40 and 41.

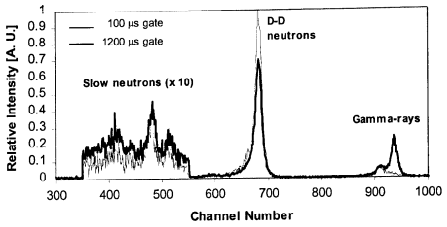


Figure 39. Gated TOF spectra obtained in the bombardment of the target charged with deuterium gas at 1 bar at room temperature, with 5 MeV deuteron beam. Gates of two different widths and delays were applied.

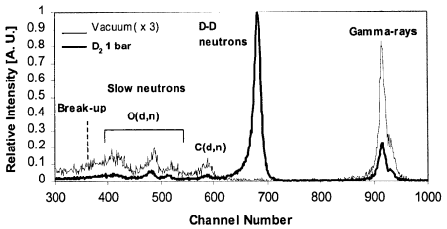


Figure 40. Gated TOF spectra obtained in the bombardment of evacuated target and target charged with deuterium gas at 1 bar at room temperature, with a 5 MeV deuteron beam.

In Figure 40 the gated TOF spectra were obtained with a 5 MeV deuteron beam incident on a gas target that was first evacuated and than charged with deuterium gas at 1 bar.

Clearly, there are 5 components in the slow neutron background corresponding to maximum neutron energies of 4.2, 3.1, 2.8 and 1.9 MeV. As the residual air was a likely contaminant of the target gas, the TOF spectra for different air / deuterium gas mixtures were obtained in order to observe any change in spectral shape (Figure 41). It is evident that increasing the air contamination resulted in decreased fast neutron yield and increased background neutron as well as gamma-ray production.

The three neutron groups resulting from the $^{16}O(d,n)^{17}F$ reaction (Q = - 1.625 MeV), corresponding to maximum neutron energies of 3.1, 2.8 and 2.3 MeV are clearly seen in the spectra in Figure 40 and in

Figure 41. The neutron group with the maximum energy at 4.2 MeV results from the $^{12}C(d,n)^{13}N$ reaction, while the lowest energy neutron group at 1.9 MeV results from deuteron break-up processes.

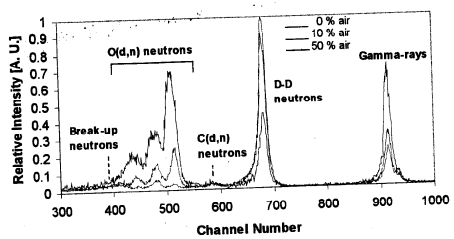


Figure 41. Gated TOF spectra obtained in the bombardment of the target charged with deuterium gas contaminated with air, with a 5 MeV deuteron beam.

The gamma-rays are generated during the beam pulse, when the beam hits the steel construction of the target box, the rotating disc seal or the Ta end-stop of the target. In order to measure the gamma-ray yield, the TOF-gated gamma-ray energy spectra were obtained from the bombardment of the evacuated gas cell with a stationary disc seal, with a 5 MeV deuteron beam. The position of the disc seal was first chosen so that the gas cell entrance aperture was obstructed and the entire incident beam was stopped in the steel material of the disc seal. Next, a hole in the disc seal was aligned with the entrance aperture of the gas cell allowing for the beam to be transported to the Ta end-stop. The resulting gamma-ray spectra are presented in Figure 42.

More than an order of magnitude decrease in gamma-ray yield is evident when the beam is stopped on the Ta end-stop. Both spectra are dominated by the strong 511 keV line. Characteristic gamma-ray lines are marked in keV (numbers in bold type indicate characteristic emission from steel). A fraction of the incident beam struck the steel material of the disc seal and therefore, some gamma-ray lines characteristic to steel appear in the 'Ta' spectrum.

When bombarded with a suitably pulsed 5 MeV deuteron beam, the target system consisting of 3 cm long gas cell charged with deuterium gas at 1 bar at room temperature, produced fast neutrons with the maximum energy of 8.2 MeV, with a spread of 180 keV. The measured 0° neutron yield was ~ 10^8 n sr^{-1} μC^{-1}. The slower neutron (E_n < 4.5 MeV) yield was 0.8 x 10^7 n sr^{-1} μC^{-1} and the gamma-ray yield (450 keV < E_γ < 8192 keV) was 0.9 x 10^7 photons sr^{-1} μC^{-1}.

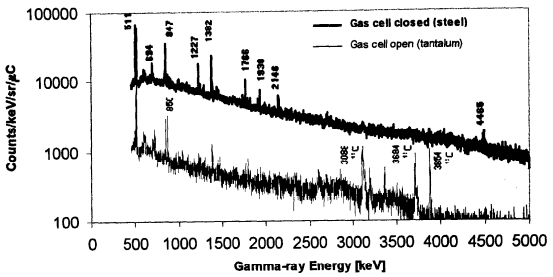


Figure 42. TOF-gated gamma-ray spectra obtained in the bombardment of the evacuated target with stationary disc seal, with a 5 MeV deuteron beam. Positions of the disc seal correspond to the full opening of the gas cell (the beam dumped on Ta end-stop) and to the fully obscured gas cell by the disc seal (the beam dumped on steel).

The neutron energy spread can be tailored to a specific application by varying the gas cell length or adjusting the target gas pressure, while the neutron yield of the target is only limited by the heat dissipation capability of the end-stop and the beam current of the accelerator. The use of deuteron beams with an average power of 500 W is possible with a simple water-cooled Ta end-stop.

6.2.3 Conclusions

The feasibility of a relatively compact, high pressure windowless target for mono-energetic neutron production has been demonstrated. The rotating disc seal concept allows for reliable operation of the target with a target gas pressures in excess of 1 bar. This gas target is the best suited for operation with low duty cycle accelerators such as the RFQ linacs.

The beam handling capabilities of the target are only limited by the heat dissipation at the end-stop of the target cell. A simple design of the water-cooled tantalum end-stop tolerates in excess of 500 W of the beam power (100 μA of a 5 MeV deuteron beam).

The differentially pumped deuterium gas target with a 3 cm gas cell was tested at the target gas pressure of 1 bar with a 5 MeV deuteron beam. It produced 8.2 MeV neutrons with a spread of 200 keV at 0° with the measured output of 10^8 n sr^{-1} μC^{-1}.

The slow neutron background resulting from deuteron break-up and contamination of the target gas, and the gamma-rays resulting from the interaction of the particle beam with the construction materials of the target, contributed 6.8 % and 7.7 % to the total reaction yield, respectively.

The design of the differentially pumped gas target described above presents a relatively simple solution to the production of high fluxes of mono-energetic fast neutrons. The mono-energetic neutron output of this gas target at 0° can exceed 10^{12} n sr^{-1} s^{-1}, when used with accelerators capable of the particle beam currents of the order of 1 mA, with the minimum contamination from gamma rays and slow neutrons. This should open possibilities for further development for a number of applications, to date limited by the neutron source strength, including elemental fast neutron radiography.

7. CONCLUSIONS

This work demonstrates the feasibility of resonant fast neutron radiography for applications in the industrial environment. An element-sensitive fast neutron probe can be designed to exploit the resonant structure of the fast neutron excitation function for the element of interest.

Commercially available compact accelerators such as cyclotrons or RFQ linacs, operating at relatively low energy and are the best suited accelerator-based fast neutron source for industrial applications. The fast neutron spectrum can be application-tailored by the appropriate design of the accelerator and the selection of a suitable nuclear reaction. The most of fast neutron applications are limited by the neutron source output. This limitation is particularly severe when mono-energetic neutron sources are required. Therefore, high current accelerators (> 1 mA) need to be employed in order to achieve the suitably short probing and analysis times.

The suitable targets need to be developed for use with these accelerators. Such targets are required to be able to tolerate up to 50 kW of particle beam power and to produce a fast neutron flux of the desired spectrum with a minimum gamma-ray and slow neutron component. This is a particularly strict requirement for the gaseous targets, such as used in popular (D,D) and (D,T) reactions. This thesis proposes a solution to the problem if a pulsed accelerator is used. However, the recently reported experiments of Hershcovitch [138, 139] indicate that it may be possible to create a stabilised plasma arc as an interface between the accelerator vacuum and the high pressure region of the gas target, which can be used with a continuous beam. Such a plasma porthole may remove all limitations on beam current, energy and energy focussing that are common for solid window targets.

Future research should concentrate on the techniques of detection of the fast neutrons in the image format. The very low neutron detection efficiency of the currently available scintillating screens make the utilization of fast neutron beams, generated at the neutron source, extremely ineffective. Furthermore, the additional loss of signal takes place in CCD-based imaging detectors due to optical minification of the light image during its transfer to the CCD array. Clearly, better scintillating screen concept and new imaging detector design would benefit fast neutron radiography applications.

Neutron detection efficiency of a scintillating screen can be easily increased by increasing its thickness. This approach however, results in a degradation of spatial resolution and can be applied in radiography to a limited degree only. In the case of ZnS-based scintillators the maximum effective thickness (~ 1 mm) is already limited by the opacity of the material to its own light.

A several centimeter thick plastic scintillators are free of this last limitation and offer good neutron detection efficiency with improved spatial resolution, when used as a fiber bundle. The spatial resolution can be further improved if the orientation of fibers is such that it matches the angular divergence of the neutron beam.

An alternative approach could use an array of capillaries filled-up with an organic liquid having high hydrogen-to-carbon (H/C) ratio. The technology used in the manufacturing of micro-channel plates for image intensifiers can be investigated, while there are various liquid scintillators having high H/C ratio (H/C ratio of 2 is available [75]).

The small size of the CCD arrays, typically 10-15 mm square, usually requires the optical minification of the original image recorded in a scintillator. This results in a significant signal loss, depending on the degree of minification (Lambertian radiator) and degrades the detectability in an image. In addition, the CCD structures are prone to radiation damage due to neutron and gamma-rays which results in gradual degradation of the image quality.

The large flat panel image sensors, based on the thin film transistor (TFT) amorphous silicon (A-Si) technology are becoming commercially available [140]. These detectors, developed primarily for medical imaging applications have many potential advantages for applications in fast neutron radiography. The typical size of the A-Si plate is 200 x 200 mm, with a pixel size of 127 μm, which allows for close coupling of the scintillating screen with no optics required and consequently, no signal loss. The detector typically offers a 12-bit dynamic range, 4 lp/mm resolution and low electronic noise. In addition, the A-Si detector is more radiation-resistant due to the amorphous structure of the image sensing area. The above mentioned advantages of the A-Si imaging detector merit a careful evaluation of the suitability of this detector in fast neutron radiography applications.

Finally, novel imaging techniques, such as time-of-flight radiography [141], need to be investigated. Accelerator-based fast neutron radiography often suffers from undesirable interference such as accompanying gamma-ray fields and low energy neutrons resulting from the complexity of the nuclear reaction employed for neutron production. Hence, the use of an integrating detector such as CCD may lead to significant contrast degradation if, as usually is the case, the primary fast neutron beam constitutes only a fraction of the total beam generated. On the other hand, the different components of the beam usually carry highly complementary information, if it can be resolved in an image.
This can practically be achieved if a nano-second pulsed fast neutron source is used with a CCD detector coupled to a fast gated image intensifier, acting as an opto-electronic shutter. The detector can then be triggered on the selected part of the TOF spectrum, effectively separating gamma-ray, fast neutron and slow neutron components of an image. Furthermore, the effects of scattered and secondary radiation can also be significantly minimized. The mono-energetic neutron imaging can in principle be achieved with white neutron sources, by proper use of the time-structure of the beam.

The promising results of this project as well as clear and reasonably achievable objectives of future research, may ensure a wider application of elemental fast neutron imaging in solving various industrial problems.

REFERENCES

[1] U. A. S. Tapper and J. Guzek, 'Particle Analysis and Sorting', SA Patent 93/6657.

[2] U. A. S. Tapper, J. Guzek, J. I. W. Watterson and H. Rahmanian, 'Method and Apparatus for the Classification of Particulate Matter', SA Patent 93/9617.

[3] U. A. S. Tapper, J. Guzek and S. N. Surujhlal, 'Method and Apparatus for the Classification of Matter', SA Patent 94/0098.

[4] U. A. S. Tapper, G. W. Over, J. Guzek, H. Rahmanian and J. I. W. Watterson, 'Scintillator Detector', SA Patent 95/5218.

[5] U. A. S. Tapper, J. Guzek and J. I. W. Watterson, 'Neutron Beam Generator', SA Patent 95/7686.

[6] U. A. S. Tapper and R. W. Hamm, 'Production of Energy Modulated Fast Neutron Beam', SA Patent 96/1730.

[7] K. Richardson, U. A. S. Tapper, J. Guzek and J. I. W. Watterson, 'Neutron Radiography Gas Target', SA Provisional Patent H0613.224.

[8] M. C. Underwood and J. S. Petler, 'Bulk Material Analysis Using Energetic Neutrons', Nuclear Geophysics, Vol. 1, No. 3, pp. 235-241, 1987.

[9] G. Vourvopoulos, 'Industrial on-line bulk analysis using nuclear techniques', Nuclear Instruments and Methods in Physics Research B56/57 (1991) 917-920.

[10] H. R. Cooper, 'Advances in on-line particulate composition analysis', Powder Technology, 69 (1992) 93-99.

[11] C. G. Clayton and J. S. Schweitzer, 'A Review of Aspects of Nuclear Geophysics', Nuclear Geophysics, Vol. 7, No. 2, pp. 143-171, 1993.

[12] J. I. W. Watterson and H. Rahmanian, 'Potential for an accelerator-based neutron source for the logging of bore-hole cores', Nuclear Instruments and Methods in Physics Research B79 (1993) 571-573.

[13] N. G. Cutmore, B. D. Sowerby and J. S. Watt, 'On-line Analysis of Coal', Nuclear Geophysics, Vol. 7, No. 4, pp. 519-528, 1993.

[14] J. I. W. Watterson, 'Optimisation of geometrical and spectral factors for the determination of carbon in coal by neutron-induced prompt gamma-ray analysis', Nuclear Geophysics Vol. 7 (1993) 87-95.

[15] M. Borsaru, 'Nuclear Techniques for In Situ Evaluation of Coal and Mineral Deposits, Nuclear Geophysics, Vol. 7, No. 4, pp. 555-574, 1993.

[16] J. I. W. Watterson, Report SRCNS 86/03, Schonland Research Centre, University of the Witwatersrand, Johannesburg, April, 1986.

[17] J. I. W. Watterson, A. E. Pillay and P. Nailand, 'Selective activation analysis with ion-beam-tailored neutron spectra – a comparison between the reactions $^{7}Li(p,n)^{7}Be$ and $^{9}Be(p,n)^{9}B$',Nuclear Instruments and Methods in Physics Research B45 (1990) 75-80.

[18] T. K. Magagula and J. I. W. Watterson, 'The excitation of isomeric states by accelerator neutrons from the $^{7}Li(p,n)^{7}Be$ reaction and their application in selective application analysis', Proceedings of the 5th European Conference on Accelerators in Applied Research and Technology, Eindhoven, August 1997.

[19] L. Grodzins, 'Nuclear techniques for finding chemical explosives in airport luggage', Nuclear Instruments and Methods in Physics Research B56/57 (1991) 829-833.

[20] L. Grodzins, 'Detecting contraband in luggage', Nuclear Instruments and Methods in Physics Research B79 (1993) 597-600.

[21] T. Gozani, 'Neutron based non-intrusive detection techniques', Proceedings International Conference 'Neutrons in Research and Industry', 9-15 June 1996, Crete, Greece, ed. G. Vourvopoulos, SPIE Proceedings Series, Vol. 2867, pp. 174-181.

[22] R. E. Schefer, R. E. Klinkowstein and J. C. Yanch, 'High-current electrostatic accelerator for boron neutron capture therapy', Proceedings International Conference 'Neutrons in Research and Industry', 9-15 June 1996, Crete, Greece, ed. G. Vourvopoulos, SPIE Proceedings Series, Vol. 2867, pp. 41-47.

[23] B. A. Ludewigt, W. T. Chu, R. J. Donahue, J. Kwan, T. L. Phillips, L. L. Reginato and R. P. Wells, 'An Epithermal Neutron Source for BNCT Based on an ESQ-Accelerator', Proceedings of the Annual Meeting of the American Nuclear Society, Albuquerque, NM, November 16-20, 1997, to be published.

[24] C-O. Fisher, 'The History of the First Neutron Radiographs in Berlin 1935-1944, Neutron Radiography Proceedings of the Fourth World Conference, San Francisco, California, 1992, pp. 3-9.

[25] Neutron Radiography Proceedings of the First World Conference, San Diego, California, USA, December 7-10, 1981, ed. J. P. Barton and P. von der Hardt, D. Reidel Publishing Company.

[26] Neutron Radiography Proceedings of the Second World Conference, Paris, France, June 16-20, 1986, ed. J. P. Barton, G. Farny, J-L. Person and H. Rottger, D. Reidel Publishing Company.

[27] Neutron Radiography Proceedings of the Third World Conference, Osaka, Japan, May 14-18, 1989, ed. S. Fujine, K. Kanda, G-I. Matsumoto and J. P. Barton, D. Reidel Publishing Company.

[28] Neutron Radiography Proceedings of the Fourth World Conference, San Francisco, California, 1992.

[29] Proceedings Fifth World Conference on Neutron Radiography, June 17-20, 1996, Berlin, Germany, ed. C. O. Fischer, J. Stade and W. Bock, Deutsche Gesselschaft fur Zerstorungsfreie Prufung E. V.

[30] D. K. Bewley, M. Catterall and B. C. Page, 'Medical Radiography with Fast Neutrons, British Journal of Radiology, Vol.46, No. 541, 1973.

[31] R. Becker and G. Hehn, 'Radiography with Fast Neutrons', Atomkernenergie, Vol. 26, 1975.

[32] J. C. Overley, 'Element-sensitive Computed Tomography with Fast Neutrons', Journal of Computer Assisted Tomography, 7(1), pp. 117-125, 1983.

[33] J. C. Overley, 'Element-sensitive Computed Tomography with Fast Neutrons', IEEE Transactions on Nuclear Science, Vol. NS-30, No. 2, 1983.

[34] J. C. Overley, 'Element-sensitive Computed Tomography with Fast Neutrons', Nuclear Instruments and Methods in Physics Research B24/25 (1987) 1058-1062.

[35] E. Duhmke, L. Greim and H-W. Schmitz, 'Fast Neutron Radiography (FNR) with track etch technique', Neutron Radiography Proceedings of the Second World Conference, Paris, France, June 16-20, 1986, ed. J. P. Barton, G. Farny, J-L. Person and H. Rottger, D. Reidel Publishing Company, pp. 639-646.

[36] E. Duhmke and L. Greim, 'Medical Radiography with Fast Neutrons in Radiotherapy', Neutron Radiography Proceedings of the Third World Conference, Osaka, Japan, May 14-18, 1989, ed. S. Fujine, K. Kanda, G-I. Matsumoto and J. P. Barton, D. Reidel Publishing Company, pp. 687-694.

[37] A. K. Schatz, G. Pfister, D. Koch, G. Stier and C. Siegel, 'Computer-Tomography with Fast and Thermal Neutrons', Neutron Radiography Proceedings of the Third World Conference, Osaka, Japan, May 14-18, 1989, ed. S. Fujine, K. Kanda, G-I. Matsumoto and J. P. Barton, D. Reidel Publishing Company, pp. 805-812.

[38] G. Pfister, A. K. Schatz, C. Siegel, E. Steichele, W. Waschkowski and T. Buchel, 'Nondestructive Testing of Materials and Components by Computerized Tomography with Fast and Thermal Reactor Neutrons', Nuclear Science and Engineering 110 (1992), pp. 303-315.

[39] G. Pfister, A. K. Schatz, J. Gobel and R. Kofler, 'Computerized Tomography with Fast and Thermal Neutrons State of the Art and Future Perspectives', Proceedings International Symposium on Computerized Tomography for Industrial Applications, Berlin, Germany, 8-10 June 1994.

[40] T. G. Miller and W. H. Makky, 'Application of Fast Neutron Spectroscopy/ Radiography to Airport Security', SPIE, Vol. 1737, 1992, pp. 184-196.

[41] T. G. Miller, 'Use of Neutron Tomography for Airline Security', Proceedings of SPIE International Symposium on Substance Identification Technology, Innsbruck, Austria, SPIE, Vol. 2093, 1993, pp. 204-217.

[42] R. Loveman, E. Pentaleri and T. Gozani, 'Nuclear resonance Techniques for Drug and Explosive Inspection in Luggage', Proceedings of Counterdrug Law Enforcement: Applied Technology for Improved

Operational Effectiveness International Technology Symposium, Nashua, New Hampshire, 1995, pp. 10-53 – 10-63.

[43] R. A. Loveman, R. L. Feinstein, J. Bendahan, T. Gozani and P. Shea, 'Laminography Using Resonant Neutron Attenuation for Detection of Drugs and Explosives, Proceedings of the Fourteenth International Conference Application of Accelerators in Research and Industry, Denton, Texas, 1996, ed. J. L. Duggan and I. L. Morgan, American Institute of Physics Conference Proceedings 392.

[44] G. F. Knoll, 'Radioisotope Neutron Sources',S. 'Neutron Sources for Basic Physics and Applications', ed. S. Cierjacks, Pergamon Press, 1983, pp. 7-18.

[45] J. Csikai, 'Utilisation of Intnse neutron generators in Science and Technology', Nuclear Instruments and Methods in Physics Research A280 (1989) 233-250.

[46] M. Drosg, 'Sources of Variable Energy Monoenergetic Neutrons for Fusion Related Applications', Nuclear Science and Engineering 106 (1990), pp. 279-280.

[47] G. S. Bauer, 'The Spallation Neutron Source SINQ', Paul Scherer Institut, October 1994.

[48] G. Peto and R. Pepelnik, 'High-Intensity 14 MeV Deuterium-Tritium Neutron Generators: Present Achievements and Future Potentials', Nuclear Science and Engineering 106 (1990), pp. 219-227.

[49] R. W. Hamm, 'Neutron Production with Compact Ion Linacs', Proceedings International Conference 'Neutrons and Their Applications', 12-18 June 1994, Crete, Greece, ed. G. Vourvopoulos and T. Paradellis, SPIE Proceedings Series, Vol. 2339, pp. 170-174.

[50] Y. Jongen, T. Delvigne and P. Cohilis, 'Multi-miliampere Compact Cyclotrons Used as Neutron Sources', Proceedings International Conference 'Neutrons and Their Applications', 12-18 June 1994, Crete, Greece, ed. G. Vourvopoulos and T. Paradellis, SPIE Proceedings Series, Vol. 2339, pp. 225-233.

[51] J. E. Brolley, Jr and J. L. Fowler, 'Fast Neutron Physics', Interscience Publishers, 1960.

[52] C. A. Uttley, 'Sources of Monoenergetic Neutrons', Neutron Sources for Basic Physics and Applications, ed. S. Cierjacks, Pergamon Press, 1983, pp. 19-57.

[53] J. Csikai, 'CRC Handbook of Fast Neutron Generators', Boca Raton, Florida, 1987.

[54] M. Drosg, 'Properties of Monoenergetic Neutron Sources from Proton Reactions with Nuclei Other Than Tritons, Proceedings IAEA Consultants Meeting on Neutron Source Properties, Debrecen, Hungary, 1980, pp. 241-264, IAEA Int. Nucl. Data Comm. Report INDC (NDS) – 114/GT ed. K. Okamoto.

[55] M. Drosg and O. Schwerer,' Production of Monoenergetic Neutrons Between 0.1 and 23 MeV', Handbook on Nuclear Activation Data, ed. K. Okamoto, pp. 81-162, IAEA Technical Report Series 273, Vienna, Austria, 1987.

[56] J. K. Bair, C. M. Jones and H. B. Willard, 'Neutrons from proton bombardment of ^{6}Li, ^{7}Li, ^{9}Be, ^{11}B, and ^{18}O', Nuclear Physics, Vol. 53, 1964, pp. 209-218.

[57] M. Drosg, 'Updating Survey of Some Less Common Fast Neutron Sources: ^{9}Be(p,n)^{9}B, ^{11}B(p,n)^{11}C, ^{51}V(p,n)^{51}Cr and ^{9}Be(α,n)^{12}C', IAEA Report IAEA-TECDOC-410, 1987, pp. 285-295.

[58] P. Grand and A. N. Goland, 'An Intense Neutron Source Based Upon the Deuteron Stripping Reaction', Nuclear Instruments and Methods in Physics Research Vol. 145 (1977) 49-76.

[59] M. A. Lone, C. B. Bingham, J. S. Fraser, H. R. Schneider, T. K. Alexander, A. J. Fergusson and A. B. McDonald, 'Thick target neutron yields and spectral distributions from the ^{7}Li($^{d}_{p}$,n) and ^{9}Be($^{d}_{p}$,n) reactions', Nuclear Instruments and Methods in Physics Research, Vol. 143 (1977), 331-344.

[60] M. A. Lone, A. J. Ferguson and B. S. Robertson, 'Characteristics of Neutrons from Be Targets Bombarded with Protons, Deuterons and Alpha Particles', Nuclear Instruments and Methods in Physics Research, Vol. 189 (1981) 515-523.

[61] T. Inada, K. Kawachi and T. Hiramoto, 'Neutrons from Thick Target Beryllium (d,n) Reactions at 1.0 MeV to 3.0 MeV', J. of Nucl. Sci. and Tech., Vol. 5(1), pp 22-29, 1968.

[62] S. Whittlestone, 'Neutron Distribution from the Deuteron Bombardment of a Thick Beryllium Target', J. Phys. D: Appl. Phys., Vol. 10, pp 1715-1723, 1977.

[63] D. L. Smith, J. W. Meadows and P. T. Guenther, 'Neutron Emission from the ^{9}Be(d,n)^{10}B Thick-Target Reaction for 7 MeV Deuterons', Nuclear Instruments and Methods in Physics Research A241 (1985) 507-510.

[64] F. M. Baumann, G. Domogala, H. Freiesleben, H. J. Paul, S. Puhlvers and H. Sohlbah, 'The ^{9}Be(d,n)^{10}B-Reaction as Intense Neutron Source with Continuous Energy Spectrum', Nuclear Instruments and Methods, A247 (1986), 359-366.

[65] J. W. Meadows, 'The ^{9}Be(d,n)^{10}B Thick Target Neutron Spectra for Deuteron Energies Between 2.6 and 7.0 MeV', Nuclear Instruments and Methods in Physics Research, A324 (1993) 239-246.

[66] J. Guzek, U. A. S. Tapper, W. R. McMurray and J. I. W. Watterson, 'Characterisation of the ^{9}Be(d,n)^{10}B reaction as a source of neutrons employing commercially available radio frequency (RFQ) quadrupole linacs, Proceedings International Conference 'Neutrons in Research and Industry', 9-15 June 1996, Crete, Greece, ed. G. Vourvopoulos, SPIE Proceedings Series, Vol. 2867, pp. 509-512.

[67] J. I. W. Watterson, R. C. Lanza, J. Guzek, W. R. McMurray, E. Iverson and U. A. S. Tapper, 'Small deuteron accelerator as a source of slow neutrons', Proceedings International Conference 'Neutrons in Research and Industry', 9-15 June 1996, Crete, Greece, ed. G. Vourvopoulos, SPIE Proceedings Series, Vol. 2867, pp. 533-536 .

[68] W. B. Howard, S. M. Grimes, T. N. Massey, S. I. Al-Quaraishi, D. K. Jacobs, C. E. Brient and J. C. Yanch, 'Thick target neutron spectrum from the ^{9}Be(p,n) reaction', Proceedings International Conference 'Neutrons in Research and Industry', 9-15 June 1996, Crete, Greece, ed. G. Vourvopoulos, SPIE Proceedings Series, Vol. 2867, pp. 84-87.

[69] J. Guzek, W. R. McMurray, C. B. Franklyn, T. Mateva and U. A. S. Tapper, 'Characterisation of neutron and gamma emission from bombardment of Beryllium with protons with kinetic energies below 10 MeV', 42nd Annual Conference of South African Institute of Physics, Durban, July 1997.

[70] J. Guzek, W. R. McMurray, T. Mateva, C. B. Franklyn and U. A. S. Tapper, 'Characterisation of neutron and gamma-ray emission from thick, Be(p,n) reaction for boron neutron capture therapy', Proceedings of ECAART5, Eindhoven, The Netherlands, 26-30 August, 1997, accepted for publication in Nuclear Instruments and Methods in Physics Research B 139 (1998) 471-475.

[71] M. Drosg, 'Sources of Fast monoenergetic neutrons. Most recent development.', Proceedings International Conference 'Neutrons and Their Applications', 12-18 June 1994, Crete, Greece, ed. G. Vourvopoulos and T. Paradellis, SPIE Proceedings Series, Vol. 2339, pp. 145-155.

[72] M. Drosg, 'Monoenergetic neutrons in the energy range from 100 eV to 200 MeV from two-body reactions with the hydrogen nuclei', Proceedings International Conference 'Neutrons in Research and Industry', 9-15 June 1996, Crete, Greece, ed. G. Vourvopoulos, SPIE Proceedings Series, Vol. 2867, pp. 490-500.

[73] J. H. Neiler and W. M. Good, 'Time-of-flight Techniques', Fast Neutron Physics Part I, ed. J. B. Marion and J. L. Fowler, Interscience Publishers, 1960.

[74] J. J. Kritzinger, W. R. McMurray and R. J. Nuspliger, 'A versatile klystron bunching system for a 5.5 MV Van de Graaff accelerator', Nuclear Instruments and Methods in Physics Research, 101 (1972) 573-581.

[75] 'Scintillators for the Physical Sciences', Nuclear Enterprises, England.

[76] Detector Systems GmbH, Germany.

[77] H. Liskien and A. Paulsen, 'Neutron production cross sections and energies for the reactions ^{7}Li(p,n)^{7}Be and ^{7}Li(p,n)^{7}Be*', Atomic Data and Nuclear Tables, 15 (1975) 57-84.

[78] H. Liskien and A. Paulsen, 'Neutron production cross sections and energies for the reactions T(p,n)^{3}He and D(d,n)^{3}He', Nuclear Data Tables, 11 (1973) 569-619.

[79] H. J. Brede, G. Dietze, K. Kudo, U. J. Schrewe, F. Tancu and C. Wen, 'Neutron yields from thick Be targets bombarded with deuterons or protons', Nuclear Instruments and Methods in Physics Research, A274 (1989) 332-344.

[80] C. M. Lederer and V. S. Shirley, 'Table of the Nuclides', Wiley and Sons, New York, 1978.

[81] R. C. Byrd, C. E. Floyd, P. P. Guss and R. L. Walter, 'Cross-Section Measurement and Lane Model Analysis for the ^{9}Be(p,n)^{9}B Reaction', Nuclear Physics, A399 (1983) 94-118.

[82] K. Murphy, R. C. Byrd, C. E. Floyd, P. P. Guss and R. L. Walter, 'Measurement of $\sigma(\Phi)$ and $A(\Phi)$ for the ^{9}Be(p,n)^{9}B Reaction and Lane Model Analysis for the ^{9}Be + Nucleon System', Nuclear Physics, A455 (1986) 525-549.

[83] C. A. Kelsey, 'The Polarization of Neutrons from the ^{9}Be(p,n)^{9}B Reacttion', Nuclear Physics, 45 (1963) 235-242.

[84] J. F. Ziegler and J. P. Biersack, 'TRIM The Stopping Power and Range of Ions in Solids', Pergamon Press, New York, 1985.

[85] Lange, Munzel, Keller and Pfenning, Ta(p,n) XS.

[86] C. G. Clayton and R. Spackman, 'Neutron Intensity and Energy Distributions from Protons in the Energy Range 1.95 MeV to 5.5 MeV Incident on Thick Targets of Lithium', Int. J. Appl. Radiat. Isot. Vol. 36, No. 1, pp. 13-50, 1985

[87] F. M. Baumann, B. Bruggemann, H. Freiesleben, Th. Grodotzki and H. Chr. Hilber, 'Energy distribution and yield of neutrons from the (p,n) reaction in thick LiF targets', Nuclear Instruments and methods in Physics research A238 (1985) 443-452.

[88] H. J. Kim, W. T. Milner and F. K. McGowan, 'Nuclear Cross Sections for charged-particle-induced reactions', Charged-Particle Cross-Section Data Center, Oak Ridge National Laboratory, Oak Ridge, Tennessee, pp.225.

[89] M. Drosg, 'Accurate measurement of the counting efficiency of a NE-213 neutron detector between 2 and 26 MeV', Nuclear Instruments and Methods 105 (1972) 573-584.

[90] W. von Witsch and J. G. Willaschek, 'High-pressure gas target for the production of intense fast neutron beams', Nuclear Instruments and Methods 138 (1976) 13-17.

[91] J. M. Nitschke, 'A high intensity heavy-ion recoil-target system', Nuclear Instruments and Methods 138 (1976) 393-406.

[92] J. W. Meadows, D. L. Smith and G. Winkler, 'A high-current deuterium gas target for neutron nuclear data research', Nuclear Instruments and Methods 176 (1980) 439-442.

[93] R. J. Nickles, 'A high-pressure gas target for cyclotrons', Nuclear Instruments and Methods 177(1980) 593-594.

[94] J. D. Molitoris and J. M. Nitschke, 'Evaluation of thin metal foils as targets and windows for heavy-ion experiments', Nuclear Instruments and Methods 186 (1981) 659-662.

[95] H. Schraube, H. Johlige and A. Morhart, 'Deuterium targets as fast neutron sources on a compact cyclotron', First Symposium on Neutron Dosimetry in Biology and Medicine, Neuherber/Munchen, May 15-19, 1972.

[96] C. M. Logan, J. D. Anderson, H. H. Barschall and J. C. Davis, 'A Heavy Water Jet Target and a Beryllium Target for Production of Fast Neutrons', UCRL-76858, 1975.

[97] C. A. Kelsey, G. C. Spalek, P. M. DeLuca, G. M. Chenevert, E. C. McCullogh and R. J. Nickles, 'High Flux Fast Neutron Source for Radiation Therapy', Proceedings of the Workshop on High Intensity Neutron Generators, US Atomic Energy Commission, 1972.

[98] G. M. Chenevert, P. M. DeLuca, C. A. Kelsey and R. P. Torti, 'A tritium gas target as an intense source of 14 MeV neutrons', Nuclear Instruments and Methods 145 (1977) 149-155.

[99] C. Rolfs, J. Gorres, K. U. Kettner, H. Lorenz-Wirzba, P. Schmalbrock, H. P. Trautvetter and W. Verhoeven, 'A differentially pumped and recirculating gas target', Nuclear Instruments and Methods 157 (1978) 19-27.

[100] J. Gorres, K. U. Kettner, H. Krawinkel and C. Rolfs, 'The influence of intense ion beams on gas target densities', Nuclear Instruments and Methods 177 (1980) 295-303.

[101] E. B. Iverson, 'Windowless Gas Target for Neutron Production', PhD Thesis, Massachussets Institute of Technology, February 1997.

[102] J. Bussiere and J. M. Robson, 'A differentially pumped gas target', Nuclear Instruments and Methods 91 (1971) 103-107.

[103] J. Ulbricht, G. Clausnitzer and G. Craw, 'High density windowless gas target', Nuclear Instruments and Methods 102 (1972) 93-99.

[104] D. A. Gross and A. Melissinos, 'Production of a high density hydrogen gas jet', Nuclear Instruments and Methods 130 (1975) 1-13.

[105] J. H. Deleeuw, A. A. Haasz and P. C. Staangeby, 'Canadian Gas Target Neutron Generator Research', Nuclear Instruments and Methods 145 (1977) 119-125.

[106] D. D. Armstrong, C. R. Emigh, J. C. Hyde, E. A. Meyer and J. D. Schneider, IEEE Transactions on Nuclear Science, Vol. Ns-26, No. 3, June 1979, pp. 3055-3057.

[107] W. Tietsch, K. Bethge, H. Feist and E. Schopper, 'High density windowless gas jet target', Nuclear Instruments and Methods 158 (1979) 41-50.

[108] G. Bittner, W. Kretschmer and W. Schuster, 'A windowless high-density gas target for nuclear scattering experiments', Nuclear Instruments and Methods 167 (1979) 1-8.

[109] H. W. Becker, L. Bauchmann, J. Gorres, K. U. Kettner, H. Krawinkel, C. Rolfs, P. Schmalbrock, H. P. Trautvetter and A. Vlieks, 'A supersonic jet gas target for γ-ray spectroscopy measurements', Nuclear Instruments and Methods 198 (1982) 277-292.

[110] K. D. Bonin and T. J. McIlrath, 'Rotating disk valve for use in a differentially pumped gas system', Rev. Sci. Instrum. 55 (10), October 1994, pp. 1666-1668.

[111] J. Guzek, K. Richardson, C. B. Franklyn, A. Waites, W. R. McMurray, J. I. W. Watterson and U. A. S. Tapper, 'Development of the high pressure deuterium gas targets for the generation of intense mono-energetic fast neutron beams', submitted to Nuclear Instruments and Methods in Physics Research, June 1998.

[112] D. Hirdes, E. Georg, H. Wollnik and R. Brandt, Nuclear Instruments and Methods 130 (1975) 18.

[113] N. Jarmie, L. J. Morrison and J. C. Martin, 'Thin metal windows for gas targets', Nuclear Instruments and Methods 116 (1974) 451-452.

[114] Hamilton Precision Metals, Inc., Lancaster PA, USA.

[115] F. T. Kuchnir, F. M. Waterman and L. S. Skaggs, 'A cryogenic deuterium gas target for production of a neutron therapy beam with a small cyclotron' Proceedings of 3rd Symposium on Neutron Dosimetry in Biology and Medicine, EUR 5848 DE/EN/FR 1978, p. 369.

[116] L. S. Skaggs , F. T. Kuchnir andF. M. Waterman, 'Experience with thin havar foils for cyclotron target window'.

[117] U. A. S. Tapper and J. Guzek, De Beers Diamond Research Laboratory Internal Technical Note, TN93/02/01, February, 1993.

[118] ENDF/B-VI Summary Documentation. BNL-NCS-17541 (ENDF-201), 4th Edition ENDF/B-VI, 1991.

[119] R. E. McFarlane, D. W. Muir and R. M. Boicourt, 'The NJOY Nuclear Data Processing System, May 1982.

[120] C. B. Smith, J. I. Gurney, E. M. W. Skinner, C. M. Clement and N. Ebrahim, 'Geochemical Character of Southern African Kimberlites: A New Approach Based on Isotopic Constraints', Transactions of the Geological Society of South Africa, Vol. 88, Johannesburg, 1985.

[121] J. I. W. Watterson, Report SRCNS 97/02, Schonland Research Centre, University of the Witwatersrand, July, 1997.

[122] J. Guzek, G. Pfister, S. N. Surujhlal, T. Mateva, J. I. W. Watterson and U. A. S. Tapper, 'Modeling of fast neutron radiographic images using neutron transport codes', 41st Annual Conference of the South African Institute of Physics, Pretoria, 2-5 July, 1996.

[123] RSIC Computer Code Collection TORT-DORT Two and Three Dimensional Discrete Ordinate Transport, ver. 2.12.14, Oak Ridge National Laboratory, 14 March 1996.

[124] E. Sartori, 'Standard energy group structures of cross-section libraries for reactor shielding', Reactor Cell and Fusion Applications: VITAMIN-J, ECCO-33, ECCO-2000 and XMAS, JEF/DOC-315, June 1991.

[125] G. F. Knoll, 'Radiation Detection and Measurement', John Wiley and Sons, 1979.

[126] MCNP 4A – Monte Carlo N-Particle Transport Code System, Oak Ridge NL.

[127] T. Mateva, J. Guzek, S. Surujhlal and H. Francis, De Beers Diamond Research Laboratory Internal Technical Note, TN97/01/02, Johannesburg, January, 1997.

[128] 'LANSAR Model DL-5 Dual Energy Linac, S/N 001', Volume 1, RFQ Linac, AccSys Technology, April, 1997.

[129] M. Weiss, 'Radio-frequency quadrupole', CERN, Geneva, Switzerland.

[130] PARAMTEQ ...

[131] 'Operating and Programming Manual HP 8510B Network Analyzer', Manual Part No. 08510-90070, July 1987, Hewlett-Packard Company, USA.

[132] NEC Beam Profile Monitor Model BPM5-45, National Electrostatic Corporation, Middleton, Wisconsin, USA.

[133] K. R. Crandall and D. P. Rusthoi, 'TRACE 3-D Documentation', Second Edition, December 1990, LA-UR-90-4146, Los Alamos National Laboratory, USA.

[134] 'ICCD Detector Operation Manual', Version 2, Revision A, P/N 4411-0009, Princeton Instruments, USA.

[135] K. Yoshii, K. Miya, 'A study on the mechanism model of luminescence in fast neutron television converter', Nuclear Instruments and Methods A346 (1994) 253-258.

[136] J. Guzek, W. R. McMurray, J. I. W. Watterson and U. A. S. Tapper, 'Measurement of the total neutron cross-section using neutron time-of-flight technique', 41st Annual Conference of the South African Institute of Physics, Pretoria, 2-5 July, 1996.

[137] 'WinView User's Manual', Software Version 1.2, Manual Revision A, March 4, 1994, P/N 4411-0001, Princeton Instruments, USA.

[138] A. Hershcovitch, 'High pressure arcs as vacuum-atmosphere interface and plasma lens for nonvacuum electron beam welding machines, electron beam melting, and nonvacuum ion material modification', Journal of Applied Physics, 78 (9), 1995, 5283-5288.

[139] W. Gerber, R. C. Lanza, A. Hershcovitch, P. Stefan, C. Castle and E. Johnson,'The plasma porthole: a windowless vacuum interface with various accelerator applications", Proceedings of the Fifteenth International Conference Applications of Accelerators in Research and Industry, Denton, Texas, USA, 1998.

[140] R. E. Colbeth, M. J. Allen, D. J. Day, D. L. Gilblom, R. Harris, I. D. Job, M. E. Klausmeier-Brown, J. Pavkovich, E. J. Seppi, E. G. Shapiro, M. D. Wright and J. M. Yu, 'A Multi-mode X-ray Imager for Medical and Industrial Applications, Varian Associates, Inc.

[141] J. Guzek, C. B. Franklyn, G. Pfister, M. C. Steyn, J. I. W. Watterson, A. K. Schatz and U. A. S. Tapper, 'The feasibility of the time-of-flight fast nutron radiography'. Proceedings Fifth World Conference on Neutron Radiography, June 17-20, 1996, Berlin Germany, ed. C. O. Fischer, J. Stade and W. Bock, pp. 148.